

Cislunar Constellation Design for Space Situational Awareness with Time-Expanded Facility Location Problem

Yuri Shimane ^{*}, Kento Tomita [†], and Koki Ho [‡]
Georgia Institute of Technology, Atlanta, Georgia 30332

This work proposes a facility location problem framework for designing satellite constellations to provide Cislunar Space Situational Awareness (CSSA). The problem seeks to find the optimal locations of space-based observers to monitor a user-defined region of cislunar space, represented by a finite set of targets with potentially time-varying observation requirements. The optimization problem is posed as a time-expanded facility location problem (FLP); unlike a traditional FLP that focuses on assigning facilities to clients, the proposed formulation focuses on assigning observers to specific pointing directions from a discretized set. To aid with the solving process of the resulting large-scale binary linear program, a Lagrangean method (LM) based on constraint relaxation and custom heuristics is provided. The performance of the proposed formulation and method is demonstrated with several case studies that obtained CSSA constellations for monitoring the lunar sphere of influence, the cislunar Cone of Shame, and a transit window for low-energy transfers located in the Earth-Moon L2 neck region. The proposed problem formulation, along with the LM, is demonstrated to enable a fast assessment of near-optimal CSSA constellations.

Nomenclature

a_{diff}	= target diffusion reflectance
a_{spec}	= target specular reflectance
C_j	= set of neighbor facility locations of location j
CSSA	= Cislunar Space Situational Awareness
d	= target diameter
FLP	= Facility Location Problem
FOV	= field of view
f	= facility build cost vector

^{*}Ph.D. Candidate, Daniel Guggenheim School of Aerospace Engineering. Student Member AIAA

[†]Ph.D. Candidate, Daniel Guggenheim School of Aerospace Engineering. Student Member AIAA

[‡]Associate Professor, Daniel Guggenheim School of Aerospace Engineering. Senior Member AIAA.

LPO	=	Libration Point Orbit
i	=	pointing direction index
j	=	facility location index
\mathcal{J}	=	set of candidate facility locations
k	=	target index
\mathcal{K}	=	set of targets
ℓ	=	number of time steps
l	=	line of sight vector
M	=	visibility tensor
m	=	number of pointing directions
\bar{m}	=	apparent magnitude
n	=	number of candidate facility locations
p	=	number of facilities to be used
q	=	number of targets
r	=	position vector
t	=	time/time index
TE- p -MP	=	time-expanded p -median problem
v	=	velocity vector
X_{ijt}	=	binary variable for allocating client i to facility j at time t
Y_j	=	binary variable for using facility location j
Z	=	objective value
η_{tk}	=	Lagrange multiplier on objective equivalence constraint
λ_{jt}	=	Lagrange multiplier on single direction constraint
ϕ	=	phase angle

I. Introduction

CISLUNAR space is today's most active frontier in space exploration. In the first two months of 2024 alone, there have been two successful lunar landings, namely JAXA's SLIM and Intuitive Machines' Odysseus missions, and multiple more entities have planned launch before the end of the year. As activity in the lunar vicinity from both government and commercial players sees an unprecedented increase, the safe operation of cislunar assets necessitates a reliable infrastructure for monitoring activities of both cooperative and non-cooperative targets. Driven by this need, interest in cislunar space situational awareness (CSSA) has also seen a significant increase [1–6]. Several studies

have considered both monitoring vast cislunar regions [2, 7–13], as well as tracking specific translunar and cislunar trajectories of interest [14–17]. In particular, Wilmer et al [18, 19] and Dahlke et al [20] studied the use of libration point orbits (LPOs) for monitoring targets also located in L1 and L2 LPOs; notably, Wilmer and Bettinger [18] looked at monitoring the near-rectilinear halo orbit (NRHO), which is the planned hosting orbit for the Lunar Gateway. Finally, Patel et al [17] looked at monitoring transits from an L1 LPO to GEO.

The capability to rapidly explore the CSSA constellation design space is critical as it allows decision-makers to assess the extent to which CSSA may be conducted for a given set of monitoring demands and a given set of specifications for the observing spacecraft system. Several factors complicate the CSSA problem; one major contributor is the large number of design parameters, such as the number and location of observers, specifications of their optical sensors, requirements for the observation, and duration of the SSA activity. Another factor is the highly nonlinear dynamics and time-dependent observation conditions, which renders traditional orbital elements-based constellation design approaches inapplicable. These factors make the design of CSSA constellations complicated; to date, several works have conducted simulation-based studies on specific CSSA constellations [5, 8, 20, 21]. Vendl et al [2] presented a parametric comparison of candidate LPOs for CSSA, providing insights into the observation conditions offered by each orbit. Building on these efforts, Visonneau et al [13] posed the design as a dual-objective minimization problem, which was tackled by a variable-length genetic algorithm (GA). This formulation wrapped a simulation as part of its objective function, thereby allowing it to handle any arbitrary level of complexity in the model. Clareson et al [22] also employed a GA, and extended the realism of the simulation by considering an extended Kalman filter used to estimate the state of the observed targets. The primary drawback of these simulation-based works is the inherent, non-negligible computational cost; for example, solving a single instance of the problem in [13] took on the order of hours. Since the CSSA problem has multiple parameters and uncertainties surrounding the requirements, the slow computational performance hinders rapid assessment of the problem. Moving away from these simulation-based approaches, the work by Patel et al [17] applies the Access-profile-Pattern-Coverage (APC) decomposition scheme, originally conceived for designing Earth observation constellations [23], resulting in a binary linear program (BLP). The use of the APC allows for a much faster exploration of the trade-space, due to the existence of powerful techniques to solve BLP, primarily based on branch-and-bound (B&B) algorithms. Like many other constellation design methods, the APC decomposition scheme optimizes only the positions of the satellites; since it assumes that the satellites can view any targets within the range (i.e., no field-of-view constraints implemented), it lacks the capability to optimize the sensor pointing directions of each satellite over time considering a realistic field of view.

In broader, operations research contexts, the general class of mathematical framework for deciding the location of infrastructure assets and their assignments to clients is known as the facility location problem (FLP). FLP is a popular approach for formulating and solving location and allocation problems in terrestrial logistics applications [24–31] as well as space-based applications [32–34]. In this work, we leverage the p -median variant of the FLP, which results in a

BLP, and extend it to include the time dimension, thus accommodating the dynamic nature of motion in cislunar space. The inclusion of the time dimension into FLP is traditionally coined *multi-period* FLP (MPFLP) [35–37], where each “period” corresponds to the so-called *planning horizon* about which allocation decisions are to be made. In the context of space-based applications, the term “period” is unfortunately overloaded, as it could also denote the period of an orbit or the synodic period of the Earth-Moon-Sun system; thus, to avoid confusion with these definitions, we refer to the formulation with the time-dimension as the time-expanded p -median problem (TE- p -MP). This is also motivated by the fact that even though the MPFLP and the TE- p -MP have a mathematical resemblance, the physical meaning of a decision time step is drastically different: following the definition of strategic, tactical, and operational level decisions from Hax and Candea [38], the time-step in the TE- p -MP is at the operational level (on the order of hours), while the time-step in the MPFLP is at the strategic or tactical level (on the order of months). The MPFLP has been developed in large parts for supply chain and inventory management applications, where demands of commodities typically have predictable, seasonal fluctuations [37]. Meanwhile, to this date, the use of MPFLP in space-based applications is limited; the few exceptions include the authors’ previous works on the SSA problem [33] and on cislunar communication relays [34], where facilities have been located to discretized slots along a given set of LPOs, and allocated to observe or provide service to specific targets/clients.

In this work, we develop a TE- p -MP formulation for SSA. The novelty in the proposed formulation is twofold: firstly, at each time step, the allocation of facilities (i.e. observers) to clients (i.e. observation targets) is replaced with the allocation of facilities (i.e., observers) to directions to which the sensor is pointed. The idea of allocating observers to pointing directions rather than individual target(s) to be observed is akin to also solving the sensor tasking problem [10, 11, 39] and enables formulating the SSA problem with realistic constraints based on the field of view (FOV) of the observer’s optical sensor, without introducing a conservative capacity assumption on the number of targets it may observe at a given instance in time. Secondly, an objective function that accounts for the aggregated coverage of the target volume is defined; this avoids the optimization problem from favoring double-counting targets that are easier to observe at the cost of omitting ones that are harder to observe.

To solve the TE- p -MP, we propose a Lagrangean method (LM) based on Lagrangean relaxation along with specifically derived heuristics developed to rapidly construct feasible solutions. The combination of the TE- p -MP and the LM enables rapid optimization of CSSA constellations with no restriction on observer locations, generating a sensor pointing schedule for each observer. These TE- p -MP instances are demonstrated for SSA architectures tasked with monitoring either a static or dynamic set of predefined targets.

The remainder of this paper is organized as follows: in Section II, we provide an overview of the dynamical system in which the problem is defined, along with definitions of LPOs and LETs. This is followed by Section III, where the static and dynamic SSA demands are defined, along with the observation model adopted in this work. Sections IV and V are used to respectively introduce the various TE- p -MP instances and their Lagrangean relaxation schemes. Numerical

experiments using the proposed approach are shown in Section VI. Finally, Section VII provides conclusions to this work.

II. Dynamical Systems Preliminaries

A. Equations of Motion

In this work, the circular restricted three-body problem (CR3BP) is used to model the motion of the observer spacecraft. The frame is defined with its first axis aligned with the vector pointing from the Earth to the Moon, the third axis aligned with the angular momentum vector of the rotating motion of the two primary bodies, and the second axis completing the triad. The motion of the two primaries are assumed to be circular about their common barycenter. Let $\mathbf{x} \in \mathbb{R}^6$ denote the state of the spacecraft, composed of $\mathbf{x} = [\mathbf{r}^T, \mathbf{v}^T]^T$, where $\mathbf{r} \in \mathbb{R}^3$ denote the position of the spacecraft, $\mathbf{v} \triangleq \dot{\mathbf{r}} \in \mathbb{R}^3$ denote the velocity of the spacecraft in the rotating frame. The CR3BP equations of motion $\mathbf{f}(\mathbf{x})$ are given by

$$\begin{bmatrix} \dot{\mathbf{r}} \\ \ddot{\mathbf{r}} \end{bmatrix} = \mathbf{f}(\mathbf{x}) = \begin{bmatrix} \mathbf{v} \\ -\frac{\mu_1}{\|\mathbf{r}_1\|_2^3} \mathbf{r}_1 - \frac{\mu_2}{\|\mathbf{r}_2\|_2^3} \mathbf{r}_2 - \boldsymbol{\omega} \times (\boldsymbol{\omega} \times \mathbf{r}) - 2\boldsymbol{\omega} \times \mathbf{v} \end{bmatrix} \quad (1)$$

where $\mathbf{r}_1 \in \mathbb{R}^3$ and $\mathbf{r}_2 \in \mathbb{R}^3$ are position vectors to the first and second primary bodies with gravitational parameters μ_1 and μ_2 , and $\boldsymbol{\omega} = [0, 0, \omega]^T$ is the angular momentum vector of the Earth-Moon rotating frame. The corresponding state-transition matrix (STM) $\Phi(t, t_0) \in \mathbb{R}^{6 \times 6}$, mapping an initial linear perturbation $\delta\mathbf{x} \in \mathbb{R}^6$ at time t_0 to time t , is propagated by the initial value problem

$$\begin{cases} \dot{\Phi}(t, t_0) &= \frac{\partial \mathbf{f}}{\partial \mathbf{x}} \Phi(t, t_0) \\ \Phi(t_0, t_0) &= \mathbf{I}_6 \end{cases} \quad (2)$$

We choose canonical scales such that $\mu_1 + \mu_2 = 1$ and $\omega = 1$, the system parameters are given in Table 1.

Table 1 CR3BP parameters

Parameter	Value
Mass parameter $\mu = \mu_2$	0.01215058560962404
Length unit LU, km	389703.2648292776
Time unit TU, s	382981.2891290545
Synodic period, day	29.5

B. Libration Point Orbit

A periodic orbit is a path in state space where for some period T , $\mathbf{x}(t) = \mathbf{x}(t + T) \forall t$. In the context of CSSA, periodic orbits about the first and second libration points (L1 and L2), known as libration point orbits (LPOs), are of particular interest due to their motion residing in the cislunar region of interest.

Multiple known families of LPOs exist in the vicinity of L1 and L2; among the members of each family, a discrete subset of LPOs that have integer ratio period with respect to the synodic period T_{syn} is considered. Following convention, we denote an $M:N$ LPO as an orbit with period $T = (N/M)T_{\text{syn}}$. This is motivated by previously reported results that placing observer spacecraft on certain $M:N$ resonant LPOs with appropriate phasing is particularly beneficial for long-term SSA activity, as favorable illumination conditions become periodic [2, 13]. We note that this choice is reminiscent of opting for designing Earth observation constellations with repeating Low-Earth orbits that exhibit repeating ground tracks [23].

This work considers the synodic-resonant LPOs in the L1/L2 Lyapunov (L1/L2Ly), L2 Halo (L2HS/L2HN), Butterfly (BtfS/BtfN), Distant Prograde Orbit (DPO), and Distant Retrograde Orbit (DRO) families, with synodic resonances 1:1, 3:2, 2:1, 9:4, 5:2, 3:1, 4:1, and 9:2. This results in 40 LPOs, as shown in Figure 1. The parameters of these LPOs are given in Table 8 in Appendix VII.A. The choice of which resonant LPOs to include as candidate orbits matters if the relative positions of member satellites within a constellation must be repeated over a k -multiple of the synodic month, where k is the smallest integer such that kM/N is an integer for all considered $M:N$ ratios. This translates to whether the sought observer location and pointing schedule are only required to be transient, or if a repeating, steady-state solution is sought. With our choice of resonant LPOs, the constellation returns exactly to its initial configuration every 4 synodic months.

For each LPO, candidate observer locations, denoted by set \mathcal{J} are defined by discretizing the orbit into b *slots* equally spaced in time, where b denotes the number of slots along a given LPO. We choose b via

$$b = \text{ceil} \left(\frac{P}{\Delta t_b} \right) \quad (3)$$

where P is the period of the LPO, and Δt_b is the temporal spacing between each slot. When considering the placement of observers on an LPO, its operational cost should also be taken into account. In this work, we make use of the linear stability index of the LPO to model the station-keeping cost of operating an observer spacecraft on a given LPO. The linear stability index is given by

$$\nu = \frac{1}{2} \left| \lambda_{\max} + \frac{1}{\lambda_{\max}} \right| \quad (4)$$

where $\lambda_{\max} = \max \text{spec}\{\Phi(T, 0)\}$.

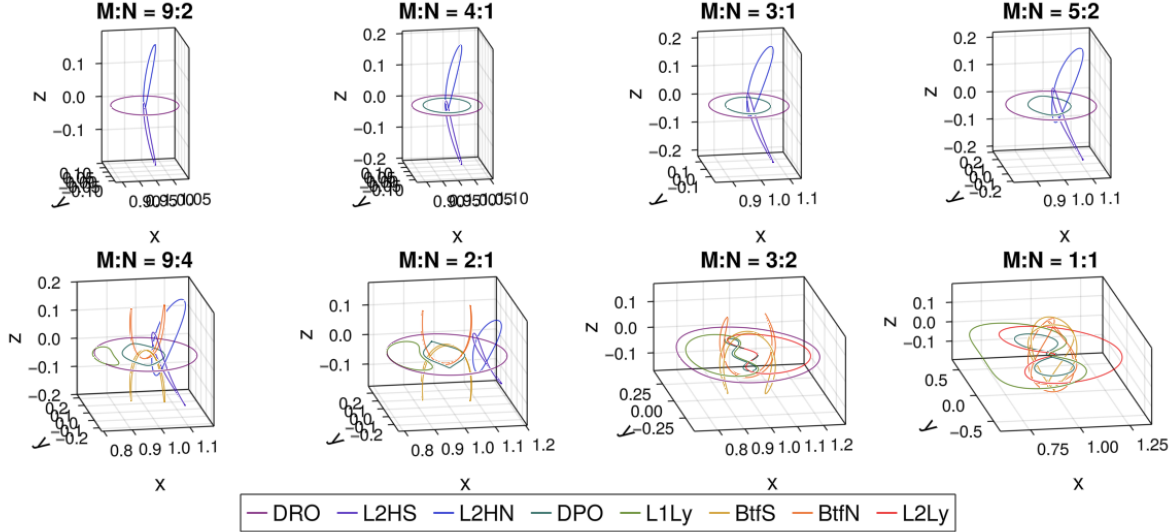


Fig. 1 Synodic-resonant LPOs considered as candidate observer orbits. For the Halo and Butterfly families, only the Southern branch is shown, but the Northern branch is also included as candidate orbits.

III. Demand and Visibility Definitions

In this Section, we introduce the demands considered for the CSSA problem. Specifically, we first distinguish between *static* and *dynamic* demands; the former consists of coverage requirement that spans the same volume over time, while the latter consists of time-dependent coverage, either to keep custody of known targets or to monitor transfer corridors that are time-dependent. In both cases, demands are defined by considering a finite set of targets distributed in space; in the static case, the demand for all targets is assumed to be always active, while in the dynamic case, the demand is activated only at time steps when the target exists. Consider $k = 1, \dots, q$ targets and $t = 1, \dots, \ell$ time steps; we define the demand matrix $D \in \mathbb{B}^{\ell \times q}$ as

$$D_{tk} = \begin{cases} 1 & \text{target } k \text{ exists at time } t \\ 0 & \text{otherwise} \end{cases} \quad (5)$$

Note that in the static case, $D_{tk} = 1$ for all t and k , while in the dynamic case, entries of D_{tk} depend on the target motions considered. Once the targets are introduced, this Section introduces the visibility model used to determine whether a given target is visible from an observer with a given solar phasing angle.

A. Static Demand

A static demand is defined by a set of targets distributed in space that remain stationary. While in reality, an object cannot remain at a fixed location in space, each “target” in this scenario may be understood as placeholders for defining a volume of interest. Then, the coverage of such a static demand translates to perpetual coverage of the volume that is

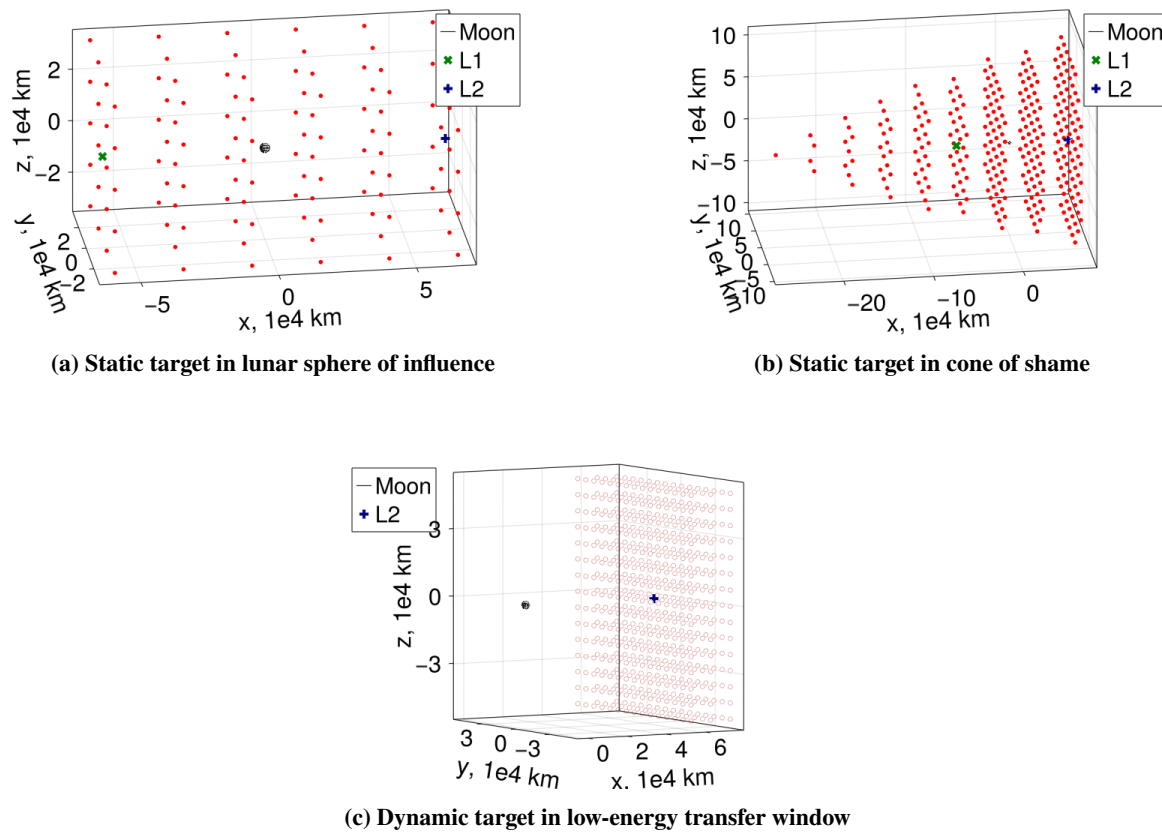


Fig. 2 Cislunar observation targets for persistent monitoring, shown in Moon-centered Earth-Moon rotating frame centered at the Moon.

spanned by the spatial distribution of these static targets.

1. Persistent Coverage of Lunar Sphere of Influence

The first static demand considered is the lunar sphere of influence (SOI). This corresponds to the lunar vicinity, where the largest number of cislunar activities, including Artemis and CLPS missions, reside after completing their respective lunar orbit injections. To define coverage demand within the lunar (SOI), an orthogonal grid of equidistant target points along each axis of the Earth-Moon rotating frame is considered. Figure 2a shows an example, with the grid spanning between Earth-Moon L1 and L2 along the x -axis, and a width and height of 6.43×10^4 km along the y - and z -axes, discretized with 6, 4, and 5 points along each respective axis, resulting in 120 targets.

2. Persistent Coverage of Cone of Shame

The so-called *cone of shame* has been coined by the Air Force Research Laboratory (AFRL) to designate the lunar exclusion zone, within which tracking objects with Earth-based sensors is particularly challenging. In this work, we consider a set of target points distributed in a cone between twice the GEO altitude and Earth-Moon L2, with a cone angle of 30° , as shown in Figure 2b, consisting of 304 targets.

B. Dynamic Demand

A dynamic demand may be defined by a variable number of targets distributed in space for any given instance in time. This formalism may be used to model the observation requirement of a specific trajectory of interest, such as that of the Lunar Gateway, or to monitor a time-varying region of interest. In this present work, we focus on the latter case, specifically looking at the persistent coverage of low-energy transfers (LETs).

1. Persistent Coverage of Low-Energy Transfer Transit Window

LETs are translunar trajectories that leverage the weak stability boundary of the Earth-Moon-Sun system to reduce the arrival specific energy with respect to the Moon at the cost of longer times of flight [40–42]. A sample set of LETs computed with the bi-circular restricted four-body model is shown in Figure 3 in the Earth-Moon rotating frame. Due to their high apogee of around 1.5 million km, LETs are hard to monitor during the majority of their transfer. Noting the fact that all LETs pass through the so-called neck region in the vicinity of Earth-Moon L2 before penetrating the cislunar vicinity, as visible on the right pane in Figure 3, we consider monitoring a volume corresponding to a transit window for LETs, centered at L2, and spanning 20 000 km along the x -axis and 100 000 km along the y/z -axes of the Earth-Moon rotating frame. The volume is represented by an orthogonal grid of 675 targets, as shown in Figure 2c. With a pre-computed database of LETs developed by the authors [33], we define D_{tk} such that the existence of the target k at a given time t is based on the existence of a LET that passes near target k at this given time. Figure 4 shows the sparsity pattern of D over four synodic periods, which repeats every synodic month, as indicated by the red lines

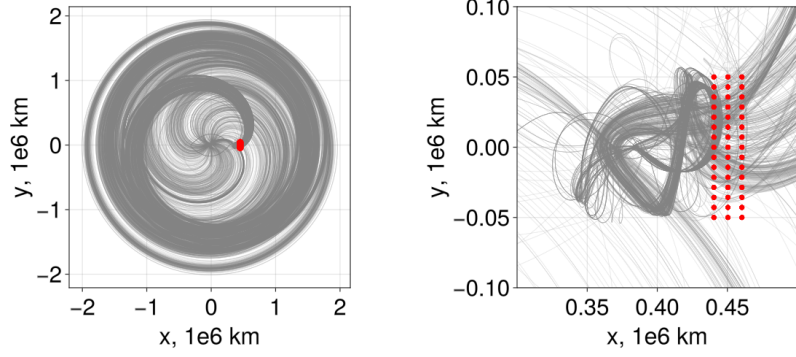


Fig. 3 200 sample LETs from pre-computed database in the Earth-Moon rotating frame centered at the Earth-Moon system barycenter. Red markers indicate transit window monitoring targets.

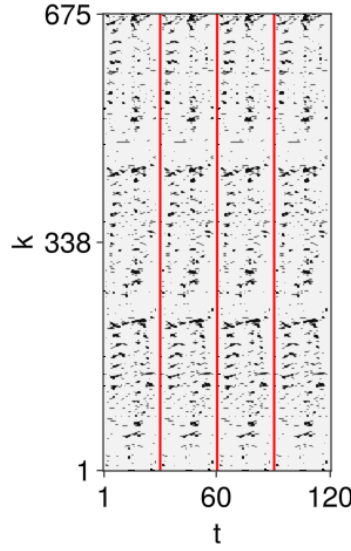


Fig. 4 Target sparsity pattern of demand matrix $D \in \mathbb{B}^{\ell \times q}$ for persistent coverage of low-energy transfer arrival window over a span of 120 time-steps lasting for four synodic months

marking the end of each month.

C. Metric for Observation Condition

The observation of a target by an observer must take into account the relative range, illumination conditions as well as the properties of both the sensor and the target. We first present the illumination model that computes the apparent magnitude of a target within the FOV of an observer, given the positions of the observer, target, and the Sun, as well as the physical properties of the target. Then, we introduce the notion of pointing directions, which considers the FOV of the observer's sensor. Finally, the above two conditions are condensed into a boolean visibility flag.

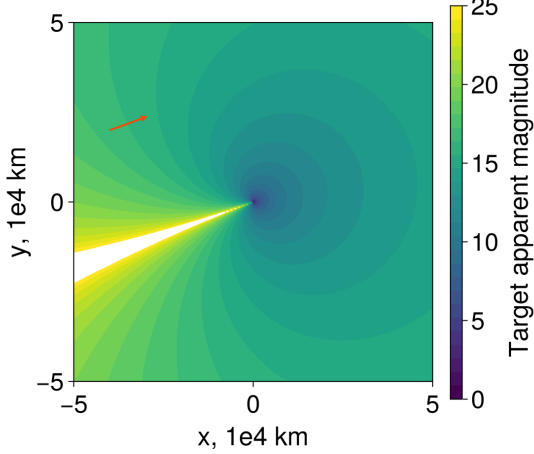


Fig. 5 Example visibility magnitude contour with $\phi_S = 200^\circ$, with Sun illumination direction aligned with orange arrow.

1. Sun Illumination Model

The Sun illumination is modeled assuming the Earth-Moon orbital plane and Sun-Earth orbital plane to be coplanar. This assumption makes the Sun, Earth, and Moon's relative geometry periodic, thus allowing for analyses to be generalized for any epoch. Note that the $\sim 5^\circ$ difference between the two planes makes a relatively small impact on the illumination conditions, thus justifying this assumption. Let $m_S = -26.74$ be the apparent magnitude of the Sun, d be the target diameter, a_{spec} be its specular reflectance, and a_{diff} be its diffusion reflectance. Furthermore, let \mathbf{r}_k denote the position vector of a target, and \mathbf{r}_j denote the position vector of an observer. Adopting the model from Vendl and Holzinger [2], the apparent magnitude of the target $\bar{m}_{\text{target}}(\mathbf{r}_j, \mathbf{r}_k)$ is given by

$$\bar{m}_{\text{target}}(\mathbf{r}_j, \mathbf{r}_k) = m_S - 2.5 \log_{10} \left(\frac{d^2}{\|\mathbf{r}_k - \mathbf{r}_j\|^2} \left[\frac{a_{\text{spec}}}{4} + a_{\text{diff}} p_{\text{diff}}(\phi_S) \right] \right) \quad (6)$$

where $p_{\text{diff}}(\phi_S)$ is the diffuse phase angle function given by

$$p_{\text{diff}}(\phi_S) = \frac{2}{3\pi} [\sin(\phi_S) + (\pi_S - \phi_S) \cos(\phi_S)] \quad (7)$$

and ϕ_S is the solar phase angle given by

$$\phi_S = \arccos \left[\mathbf{l}_{jk}^T \mathbf{l}_{Sk} \right] \quad (8)$$

where \mathbf{l}_{jk} is the unit line-of-sight vector from slot j to target k , and \mathbf{l}_{Sk} is the line-of-sight vector from the Sun to target k . Figure 5 shows the contour of \bar{m}_{target} centered at the observer, with $d = 1$ m, $a_{\text{spec}} = 0.0$ and $a_{\text{diff}} = 0.2$; the contour demonstrates the strong variation of \bar{m}_{target} with respect to ϕ_S , and the weaker variation with respect to the distance $\|\mathbf{r}_k - \mathbf{r}_j\|$ as the latter increases.

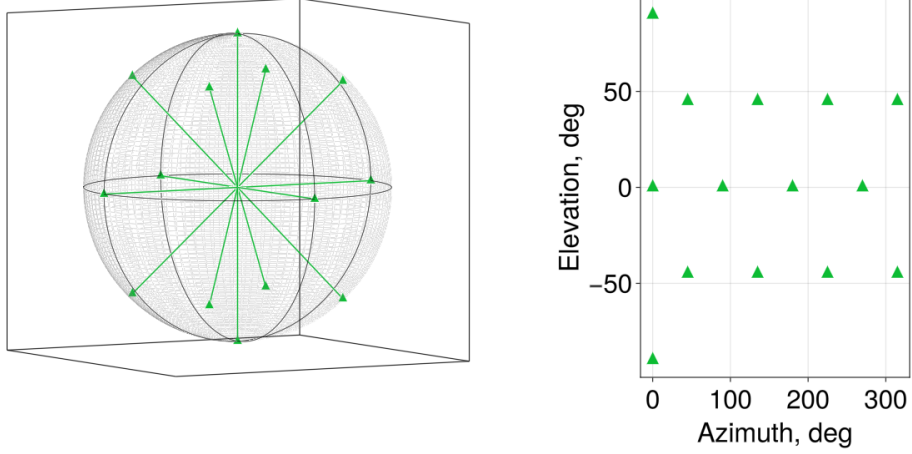


Fig. 6 Discretization of pointing directions

2. Pointing Direction

Instead of allocating observers to look at a specific target, the TE- p -MP will optimize for allocations of observers to a particular pointing direction; whether a target is visible to an observer will then depend on whether the target is within the observer's field of view. We consider a discrete set of m pointing directions, indexed by $i = 1, \dots, m$, which divides the sphere surrounding an observer into m directions, parameterized in terms of azimuth and elevation angles, α and β .

The problem of dividing a sphere into m equally distributed points is non-trivial, and suboptimal, approximation approaches such as the Fibonacci spiral may be used, especially for large numbers of m . In this work, because the TE- p -MP aims to rapidly explore the impact of different parameters of the SSA architecture, we choose to limit m to a relatively small number with easily interpreted directions. Thus, we define a set of 14 pointing directions, with 6 orthogonal directions, and 8 diagonal directions, as shown in Figure 6.

3. Visibility boolean

In this work, the emphasis is placed on whether an object is detectable at all by the sensor, rather than the optical observation quality of the target. To this end, using the expression for the apparent magnitude (6), we compute the *visibility boolean* $\bar{m}^b \in \mathbb{B}$, which denotes whether a target k is visible to an observer location j at a given time t . Three conditions must be met for an observer to be visible: firstly, the Moon must not be in occultation; secondly, the target must be in the FOV of the observer; lastly, the apparent magnitude $\bar{m}_{\text{target}}(\mathbf{r}_j, \mathbf{r}_k)$ must be below a threshold apparent

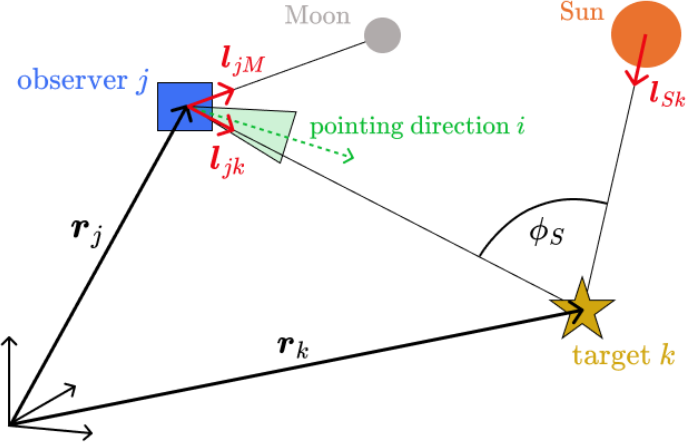


Fig. 7 Illustration of definitions used to compute the visibility boolean of a target k from an observer location j

magnitude \bar{m}_{crit} . Thus, for a given observer position $\mathbf{r}_j(t)$, target position $\mathbf{r}_k(t)$, and sensor direction $i(t)$, \bar{m}^b is given by

$$\bar{m}^b(\mathbf{r}_j(t), \mathbf{r}_k(t), i(t)) = \begin{cases} 0 & \cos^{-1}(\mathbf{l}_{jM}(t) \cdot \mathbf{l}_{jk}(t)) < \phi_{\text{Moon}}^{\text{crit}} \\ 0 & \mathbf{r}_k(t) \in \text{FOVCone}_i(\mathbf{r}_j(t)) \wedge \\ 0 & \bar{m}_{\text{target}} > \bar{m}_{\text{crit}} \\ 1 & \text{otherwise} \end{cases} \quad (9)$$

where \mathbf{l}_{jM} is the line-of-sight vector from slot j to the Moon. In equation (9), the second condition ensures the target \mathbf{r}_k is within the cone formed by the FOV from \mathbf{r}_j pointed direction i . Figure 7 shows the definitions of the quantities defined to compute the visibility boolean.

IV. Time-Expanded p -Median Problem

The traditional p -Median problem considers the problem of choosing p facilities from n candidate slots to allocate services to m clients. While the mathematical formulation developed in this work shares some resemblance to the terrestrial problem, we note that some of the physical representations of variables are different.

We consider $j = 1, \dots, n$ candidate observer locations, as is the case in the terrestrial problem. The index $i = 1, \dots, m$ denotes the candidate pointing directions for each observer to point its optical sensor. The targets are indexed by $k = 1, \dots, q$. Since the location of the observers, illumination conditions, and (depending on the considered problem) the position of the targets all move in time, an additional time index $t = 1, \dots, \ell$ is introduced. Note that, while in terrestrial FLPs, the “location” of a facility is its physical position, the “location” in space-based FLPs defines a “slot” along an orbit in which the observer spacecraft may be placed. Hence, a specific observer “location” does not refer to a fixed coordinate in space, but rather this abstract “slot” in which the observer may be placed. We use the expression

“position” to denote the physical, Cartesian coordinates of the observer at a given time.

In the remainder of this Section, we begin by introducing the design variables involved in the TE- p -MP. Then, we introduce the TE- p -MP, along with its associated coefficients, are presented.

A. Design Variables

As in the traditional FLPs, there are two sets of binary variables $X \in \mathbb{B}^{m \times n \times \ell}$ and $Y \in \mathbb{B}^n$. The variable Y dictates whether a candidate facility location is to be used, while the variable X dictates the allocation of existing facilities to clients. In the context of the CSSA problem, this allocation can be understood as an *assignment* of a facility to observe in a particular direction; furthermore, due to the dynamic nature of space, allocation decisions must be taken at each time step. The variables Y and X thus correspond to

$$Y_j = \begin{cases} 1 & \text{observer location } j \text{ is used} \\ 0 & \text{otherwise} \end{cases} \quad (10)$$

$$X_{ijt} = \begin{cases} 1 & \text{observer in location } j \text{ observes along direction } i \text{ at time } t \\ 0 & \text{otherwise} \end{cases} \quad (11)$$

B. Problem Formulation

The TE- p -MP aims to maximize the aggregated coverage of all targets across all time steps. We collect the visibility boolean $\bar{m}^b(\mathbf{r}_j(t), \mathbf{r}_k(t), i)$ from equation (9) corresponding to observer location j , pointing direction i , target k , at time t into a visibility tensor $M^b \in \mathbb{B}^{m \times n \times \ell \times q}$,

$$M_{ijtk}^b = \begin{cases} \bar{m}^b(\mathbf{r}_j(t), \mathbf{r}_k(t), i) & D_{tk} > 0 \\ 0 & D_{tk} = 0 \end{cases} \quad (12)$$

where the condition is based on whether the demand matrix D is non-zero for target k at time t . Then, the TE- p -MP is given by

$$\max_{X,Y} \quad \sum_{t=1}^{\ell} \sum_{k=1}^q \left(\max_{\substack{i=1, \dots, m, \\ j=1, \dots, n}} M_{ijtk}^b X_{ijt} \right) - \frac{1}{\ell} \sum_{j=1}^n f_j Y_j \quad (13a)$$

$$\text{s.t.} \quad \sum_{i=1}^m X_{ijt} \leq 1 \quad \forall j, t \quad (13b)$$

$$\sum_{j=1}^n Y_j = p \quad (13c)$$

$$X_{ijt} \leq Y_j \quad \forall i, j, t \quad (13d)$$

$$X_{ijt}, Y_j \in \{0, 1\} \quad \forall i, j, t \quad (13e)$$

The objective (13a) has two terms; the primary contribution comes from the first term, which maximizes the fraction of visible targets at each time-step, and takes its summation. Note that this is different from simply taking $\sum_{t=1}^{\ell} \sum_{k=1}^q \sum_{i=1}^m \sum_{j=1}^n M_{ijtk}^b X_{ijt}$, which would allow the optimizer to capitalize on observing the same target by multiple observers rather than observing as many targets as possible. The second term is a discount factor that penalizes the use of “expensive” observer locations, where $f \in \mathbb{R}^n$ is the vector of costs associated with making use of a given facility location, given by

$$f_j = 1 - \frac{1}{\nu_j + 10} \quad (14)$$

where ν_j is the stability index of the LPO, as defined by equation (4). The definition of f_j with equation (14) scales the stability index, which can take values with two orders of magnitude of difference, to values around 1. Since prohibitively expensive candidate observer locations should be excluded from the problem to begin with, it is assumed that all candidate slots are at least acceptable to be part of the solution; as such, this term is simply meant to favor combinations of facilities that are more stable in the case that multiple combinations of facilities yield the same value from the first term.

Constraint (13b) ensures each observer location j only looks to up to a single direction i at any given time t . Constraint (13c) is the traditional p -median constraint, which ensures exactly p observer is placed. Constraint (13d) is also a common constraint in the traditional p -median problem, enforcing the j^{th} observer to exist for its allocation to view direction i at time t to be used in the solution. Finally, constraint (13e) ensures the variables X and Y are binary.

The max operator in the objective (13a) may be interpreted as the infinity norm of the vector formed by concatenating all columns of the matrix $M_{:, :, tk}^b \odot X_{:, :, t}$, where \odot denotes element-wise multiplication. Then, through the introduction

of a slack variable $\theta_{tk} \in [0, 1]$ for each combination of t and k , problem (13) may be rewritten as

$$\max_{X, Y, \theta} \quad \sum_{t=1}^{\ell} \sum_{k=1}^q \theta_{tk} - \frac{1}{\ell} \sum_{j=1}^n f_j Y_j \quad (15a)$$

$$s.t. \quad \sum_{i=1}^m \sum_{j=1}^n M_{ijtk}^b X_{ijt} \geq \theta_{tk} \quad \forall t, k \quad (15b)$$

$$0 \leq \theta_{tk} \leq 1 \quad \forall t, k \quad (15c)$$

$$(13b) - (13e)$$

where constraint (15b) ensures this modified problem (15) to have the same optimal solution as the original problem (13). This is now a standard mixed-binary linear program (MBLP), which is amenable to standard solvers such as Gurobi [43] or CPLEX [44]. While the slack variable θ_{tk} is a continuous variable in $[0, 1]$, the optimal solution to (15) has $\theta_{tk} = 1$ for time t and target k if at least one observer is viewing k at this time, and $\theta_{tk} = 0$ if $\sum_{i=1}^m \sum_{j=1}^n M_{ijtk}^b X_{ijt} = 0$. Thus, this slack variable may be interpreted as a binary variable, such that

$$\theta_{tk} = \begin{cases} 1 & \text{target } k \text{ is observed by at least one observer at time } t \\ 0 & \text{otherwise} \end{cases} \quad (16)$$

For convenience in comparing obtained solutions later, we define the fraction of observation demand that has been met across all time steps, denoted as Θ , and given by

$$\Theta \triangleq \frac{\sum_{t=1}^{\ell} \sum_{k=1}^q \theta_{tk}}{\sum_{t=1}^{\ell} \sum_{k=1}^q D_{tk}} \quad (17)$$

The formulation (15) enjoys a few favorable properties; firstly, even though the slack variables θ increase the decision space, it is a continuous variable, mending itself well to standard linear program techniques. Secondly, despite the introduction of the time index t and the decomposition of allocation into pointing directions i and targets k , the general structure of the traditional p -median problem is preserved; this enables efficient use of Lagrangean relaxation, which will be introduced in Section V.

V. Lagrangean Method for the Time-Expanded p -Median Problems

One popular approach to solving complex binary linear programs (BLP) is the Lagrangean method (LM), which iteratively uses Lagrangean relaxation (LR) and problem-specific heuristics to seek the optimal solution by computing upper and lower bound solutions. The fundamental intuition behind LM is to apply LR to remove complicating constraints by adjoining them using Lagrange multipliers into the objective, in such a way that the original BLP may be

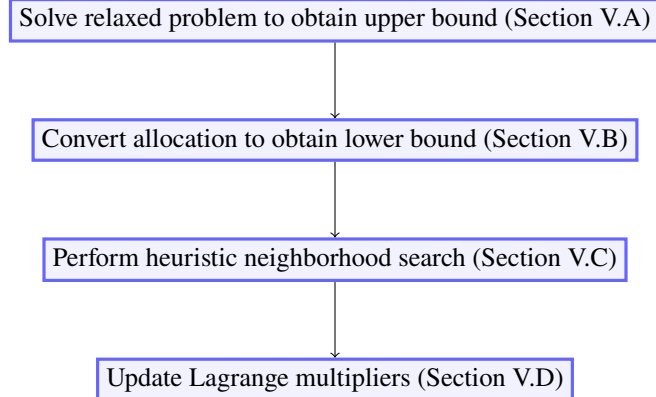


Fig. 8 Overview of a single iteration of Lagrangean method for the time-expanded p -Median problem

decoupled into smaller subproblems that are easier to solve. Since we are dealing with a maximization problem, the solution to the relaxed problem provides an upper bound of the optimal solution sought; using the solution to the LR, problem-specific heuristics are employed to generate a feasible solution, corresponding to a feasible lower bound. This process is iterated, each time updating the Lagrange multipliers towards optimality, for example using a subgradient approach.

For the p -Median problem, a popular LR is to relax constraints that pertain to allocations between i and j , resulting in decoupled subproblems corresponding to each candidate facility location j ; LR is particularly advantageous for the p -Median problem as these subproblems may be solved analytically. In this work, despite the introduction of the time indices t and slack variables θ_{tk} , we also arrive at LR expressions that achieve decomposition into subproblems corresponding to each j . We further provide a specialized set of heuristics to generate a competitive feasible lower bound solution.

In the remainder of this Section, we begin with Section V.A where we discuss the LR formulation to the original problems, along with the approach to decompose the resulting LR problem into facility-wise subproblems and to solve each of these subproblems. This is followed by Section V.B which describes the heuristic scheme devised to generate a feasible solution based on the LR solution at each iteration. An additional set of heuristics for performing a neighborhood search in an attempt to improve this feasible solution is described in Section V.C. In Section V.D, the subgradient method used to update the multipliers is introduced. The processes over one iteration of the LM are summarized in Figure 8. Finally, in Section V.E, we provide implementation considerations for implementing the proposed LM.

A. Upper Bound Solution via Lagrangean Relaxation

We specifically present the Lagrangean relaxation of the aggregated coverage problem. Relaxing constraints (13b) and (15b) with multipliers λ_{jt} and η_{tk} respectively, the Lagrangean relaxed problem is given by

$$\max_{X, Y, \theta} \quad \sum_{t=1}^{\ell} \sum_{k=1}^q \theta_{tk} - \frac{1}{\ell} \sum_{j=1}^n f_j Y_j - \sum_{j=1}^n \sum_{t=1}^{\ell} \lambda_{jt} \left(\sum_{i=1}^m X_{ijt} - 1 \right) - \sum_{t=1}^{\ell} \sum_{k=1}^q \eta_{tk} \left(\theta_{tk} - \sum_{i=1}^m \sum_{j=1}^n M_{ijtk}^b X_{ijt} \right) \quad (18a)$$

$$\text{s.t.} \quad \lambda_{it}, \eta_{tk} \geq 0 \quad \forall t, j, k \quad (18b)$$

$$(13c) \text{ -}(13e), (15c)$$

The objective may be reorganized by regrouping variables to

$$\max_{X, Y, \theta} \quad \sum_{t=1}^{\ell} \sum_{k=1}^q (1 - \eta_{tk}) \theta_{tk} + \sum_{i=1}^m \sum_{j=1}^n \sum_{t=1}^{\ell} \left(\sum_{k=1}^q \eta_{tk} M_{ijtk}^b - \lambda_{jt} \right) X_{ijt} - \frac{1}{\ell} \sum_{j=1}^n f_j Y_j + \sum_{j=1}^n \sum_{t=1}^{\ell} \lambda_{jt} \quad (19)$$

The sought optimal decision variables to the relaxed problem (18), denoted by \bar{X} , \bar{Y} , and $\bar{\theta}$ generates an upper bound to problem (15).

We first turn our attention to the slack variables θ_{tk} . Due to the relaxation of constraint (15b), the only remaining constraint on θ_{tk} is the box bound constraint (15c). Therefore, the optimal value $\bar{\theta}_{tk}$ is simply driven by its coefficient in the objective, and is trivially given by

$$\bar{\theta}_{tk} = \begin{cases} 1 & 1 - \eta_{tk} > 0 \\ 0 & \text{otherwise} \end{cases} \quad (20)$$

1. Decomposition into Subproblems

We can further recognize that this relaxation decouples the problem on a per-candidate observer location basis, where for each candidate location j , the subproblem is given by

$$\max_{X, Y_j, \theta} \quad \sum_{i=1}^m \sum_{t=1}^{\ell} \left(\sum_{k=1}^q \eta_{tk} M_{ijtk}^b - \lambda_{jt} \right) X_{ijt} - \frac{1}{\ell} (f_j Y_j) + \sum_{t=1}^{\ell} \lambda_{jt} \quad (21a)$$

$$\text{s.t.} \quad X_{ijt} \leq Y_j \quad \forall i, t \quad (21b)$$

$$X_{ijt}, Y_j \in \{0, 1\} \quad \forall i, t \quad (21c)$$

$$\lambda_{it}, \eta_{tk} \geq 0 \quad \forall t, k \quad (21d)$$

$$(15c)$$

Note that this subproblem is defined for each j , and has as variables $X_{ijt} \in \mathbb{B}^{m \times 1 \times \ell}$, $Y_j \in \mathbb{B}$, and $\theta \in \mathbb{R}^{\ell \times k}$. We denote the decision on X and Y_j made with the j^{th} subproblem as \bar{X}^j and \bar{Y}_j^j , which denote the allocations of the j^{th} observer to pointing directions over time, as well as whether the j^{th} observer should be used, respectively. We consider separately the cases where $\bar{Y}_j^j = 0$ or $\bar{Y}_j^j = 1$; the decision on whether $\bar{Y}_j^j = 0$ or $\bar{Y}_j^j = 1$ should be chosen is not made at the subproblem level, but is rather left for later when the LR solution is constructed by assembling solutions from each subproblem. If $\bar{Y}_j^j = 0$, constraint (21b) trivially forces $\bar{X}_{ijt}^j = 0 \forall i, t$. If $\bar{Y}_j^j = 1$, the choice of each $\bar{X}_{ijt}^j \forall i, t$ is driven by its coefficient in the objective, and thus the optimal value \bar{X}_{ijt}^j is given by

$$\bar{X}_{ijt}^j = \begin{cases} 1 & \sum_{k=1}^q \eta_{tk} M_{ijtk}^b - \lambda_{jt} > 0 \\ 0 & \text{otherwise} \end{cases} \quad (22)$$

The corresponding objective of the j^{th} subproblem (21a) assuming $\bar{Y}_j^j = 1$, denoted as Z_{LR}^j , is given by

$$Z_{\text{LR}}^j = \sum_{i=1}^m \sum_{t=1}^{\ell} \left(\sum_{k=1}^q \eta_{tk} M_{ijtk}^b - \lambda_{jt} \right) \bar{X}_{ijt}^j - \frac{f_j}{\ell} + \sum_{t=1}^{\ell} \lambda_{jt} \quad (23)$$

2. Construction of Lagrangean Relaxed Solution

To construct the LR solution, we first compute Z_{LR}^j for all $j = 1, \dots, n$ subproblems (21a) according to equation (23).

We then define the permutation π for the n candidate observer locations such that

$$Z_{\text{LR}}^{\pi(1)} \geq Z_{\text{LR}}^{\pi(2)} \geq \dots \geq Z_{\text{LR}}^{\pi(m)} \quad (24)$$

Then, to enforce the p -median constraint (13c), variables \bar{Y} are chosen such that the p best facilities are chosen

$$\bar{Y}_{\pi(j)} = \begin{cases} 1 & j \leq p \\ 0 & \text{otherwise} \end{cases} \quad (25)$$

Having chosen the p facility locations to be used, we construct the upper bound solution \bar{X}_{ijt} by making use of subproblem solutions \bar{X}_{ijt}^j from equation (22), such that

$$\bar{X}_{i\pi(j)t} = \begin{cases} \bar{X}_{i\pi(j)t}^{\pi(j)} & j \leq p \\ 0 & \text{otherwise} \end{cases} \quad (26)$$

Finally, the upper bound objective of the Lagrangean relaxed problem (18a) Z_{LR} is given by substituting the decision variables to equation (15a),

$$Z_{\text{LR}} = \sum_{t=1}^{\ell} \sum_{k=1}^q (1 - \eta_{tk}) \bar{\theta}_{tk} + \sum_{s=1}^p Z_{\text{LR}}^{\pi(s)} \quad (27)$$

B. Lagrangean Heuristics Reallocation

If the Lagrangean relaxed solution $(\bar{X}, \bar{Y}, \bar{\theta})$ is feasible, then it is the optimal solution (X^*, Y^*, θ^*) to problem (15). This is unlikely as constraints (13b) and (15b) have been relaxed. Thus, we seek to construct a feasible *lower* bound solution $(\underline{X}, \underline{Y}, \underline{\theta})$ using the relaxed solution. The overall procedure is summarized in Algorithm 1.

Algorithm 1 Heuristic Feasible Allocation Construction

Require: $\bar{X}, \mathcal{J}^{\bar{Y}}, M^b$

```

1:  $\underline{X} \leftarrow \bar{X}$                                 ▷ Initialize allocation variable  $X$  of feasible solution
2:  $\underline{\theta} \leftarrow \mathbf{0}_{\ell \times q}$                 ▷ Initialize slack variable  $\theta$  of feasible solution
3: for  $t = 1, \dots, \ell$  do
4:    $\mathcal{K}_t^0 \leftarrow \mathcal{K}$                       ▷ Initialize set of unobserved targets at time  $t$ 
5:    $\mathcal{J}_t^0 \leftarrow \emptyset$                       ▷ Initialize set of observers with infeasible allocations
6:   for  $j \in \mathcal{J}^{\bar{Y}}$  do
7:     if  $\sum_{i=0}^m \underline{X}_{ijt} = 1$  then
8:        $\mathcal{K}_t^0 \leftarrow \mathcal{K}_t^0 \setminus k$           ▷ Remove target  $k$  from  $\mathcal{K}_t^0$ 
9:     else
10:     $\mathcal{J}_t^0 \leftarrow \mathcal{J}_t^0 \cup \{j\}$           ▷ Append violating facility index  $j$  to  $\mathcal{J}_t^0$ 
11:     $\underline{X}_{j,t} \leftarrow 0$                          ▷ Turn all allocations of facility  $j$  at time  $t$  off
12:   end if
13:   end for
14:    $\underline{X} \leftarrow \text{GreedyAllocation}(\underline{X}, M^b, \mathcal{J}_t^0, \mathcal{K}_t^0)$           ▷ Perform allocations of facilities in  $\mathcal{J}_t^0$ 
15:   for  $t = 1, \dots, \ell, k = 1, \dots, q$  do
16:     if  $\sum_{i=1}^m \sum_{j=1}^n M_{ijtk}^b \underline{X}_{ijt} \geq 1$  then
17:        $\underline{\theta}_{tk} \leftarrow 1$                          ▷ If at least one observer is seeing target  $k$  at time  $t$ , turn  $\underline{\theta}_{tk}$  on
18:     end if
19:   end for
20: end for
21: return  $\underline{X}, \underline{\theta}$ 

```

The first step is to fix $\underline{Y} = \bar{Y}$ and initialize $\underline{X} = \bar{X}$ and $\underline{\theta} = \bar{\theta}$. Furthermore, let $\mathcal{J}^{\bar{Y}}$ denote the set of indices j that is active in \bar{Y} ,

$$\mathcal{J}^{\bar{Y}} = \{j \in 1, \dots, n \mid Y_j = 1\} \quad (28)$$

Then, we seek to satisfy constraint (13b). We begin by fixing allocations of observer location j to direction i for each time t that satisfies the constraint with an equality,

$$\underline{X}_{ijt} = \begin{cases} 1 & \sum_{i=1}^m \bar{X}_{ijt} = 1 \\ 0 & \text{otherwise} \end{cases} \quad (29)$$

and we construct the set of all targets that are unobserved at this time, \mathcal{K}_t^0

$$\mathcal{K}_t^0 = \left\{ k \in \mathcal{K} \mid \sum_{j=1}^n \sum_{i=1}^m X_{ijt} < 1 \right\} \quad (30)$$

We also record facility indices j for which the constraint at time t is violated into set \mathcal{J}_t^0 , given by

$$\mathcal{J}_t^0 = \left\{ j \in \mathcal{J}^{\bar{Y}} \mid \sum_{i=1}^m X_{ijt} \neq 1 \right\} \quad (31)$$

Equivalently, this set may be understood as the set of j that still requires allocation to an appropriate pointing direction i . The next step consists of adding back allocations for $j \in \mathcal{J}_t^0$ for each time-step t . This corresponds to the `GreedyAllocation()` functions call in line 14 of algorithm 1, and is described in further detail in the next subsection. Finally, we fix the solution to satisfy constraint (15b) by iterating through t and setting $\underline{\theta}_{tk} = 0$ if

$$\underline{\theta}_{tk} = \begin{cases} 0 & \sum_{i=1}^m \sum_{j=1}^n M_{ijtk}^b X_{ijt} = 0 \\ 1 & \text{otherwise} \end{cases} \quad (32)$$

Finally, the lower bound feasible solution Z_{LH} is given by

$$Z_{\text{LH}} = \sum_{t=1}^{\ell} \sum_{k=1}^q (1 - \eta_{tk}) \underline{\theta}_{tk} + \sum_{j=1}^n f_j Y_j \quad (33)$$

1. Greedy Allocation

In a greedy process, the facility j^* with pointing direction i^* that results in the largest additional number of targets observed is selected via the expression

$$(i^*, j^*) = \operatorname{argmax}_{\substack{i=1, \dots, m \\ j \in \mathcal{J}_t^0}} \sum_{k \in \mathcal{K}_t^0} M_{ijtk} \quad (34)$$

This process is repeated, each time setting $X_{i^* j^* t} = 1$ and removing j^* from \mathcal{J}_t^0 , until $\mathcal{J}_t^0 = \emptyset$. Algorithm 2 gives the pseudo-code for implementing this greedy allocation strategy.

2. Full-Factorial Allocation Strategy

Typically, the number of observers p in the context of the CSSA problem is relatively small, on the orders of 1s to 10s. As such, it may be computationally reasonable to spend more time sequentially allocating remaining observers $j \in \mathcal{J}_t^0$ to remaining targets \mathcal{K}_t^0 . We refer to this process as the *full-factorial* allocation; Algorithm 3 shows the pseudo-code for its procedure. The while-loop from the greedy algorithm 2 is now replaced by the outer for-loop in line 2, which iterates

Algorithm 2 Greedy Allocation

Require: $t, \underline{X}, M^b, \mathcal{J}_t^0, \mathcal{K}_t^0$

- 1: **while** $\mathcal{J}_t^0 \neq \emptyset \wedge \mathcal{K}_t^0 \neq \emptyset$ **do**
- 2: $i^*, j^* \leftarrow$ eqn. (34)
- 3: $\underline{X}_{i^*j^*t} \leftarrow 1$ ▷ Turn allocation on
- 4: $\mathcal{J}_t^0 \leftarrow \mathcal{J}_t^0 \setminus j^*$ ▷ Remove j^* from set of observers with infeasible allocations
- 5: $\mathcal{K}_t^0 \leftarrow \mathcal{K}_t^0 \setminus \{k \mid M_{i^*j^*t k}^b = 1\}$ ▷ Remove newly targets observed from set of unobserved targets
- 6: **end while**
- 7: **return** \underline{X}

through all possible permutations of indices of the set \mathcal{J}_t^0 , denoted by $\Pi_{\mathcal{J}}$. For each permutation $\pi_{\mathcal{J}} \in \Pi_{\mathcal{J}}$, we go through indices j in the order of $\pi_{\mathcal{J}}$, each time allocating j to pointing direction i in a greedy manner, such that

$$i^* = \operatorname{argmax}_{i=1, \dots, m} \sum_{k \in \mathcal{K}_t^0} M_{ijtk}^b \quad (35)$$

and targets observed by the allocation (i^*, j) are removed from \mathcal{K}_t^0 . Once the successive greedy allocation has been tried for all permutations in $\Pi_{\mathcal{J}}$, the allocations that resulted in the largest additional targets observation is returned.

Algorithm 3 Full-Factorial Allocation

Require: $t, \underline{X}, M^b, \mathcal{J}_t^0, \mathcal{K}_t^0$

- 1: $\Pi_{\mathcal{J}} \leftarrow \text{permutations}(\mathcal{J}_t^0)$ ▷ Compute permutations of j in \mathcal{J}_t^0
- 2: **for** $\pi_{\mathcal{J}} \in \Pi_{\mathcal{J}}$ **do** ▷ Iterate through each permutation
- 3: $\mathcal{K}_t^{0\pi} \leftarrow \mathcal{K}_t^0$ ▷ Make a copy of \mathcal{K}_t^0 for current permutation
- 4: $\underline{X}^{\pi} \leftarrow \underline{X}$ ▷ Make a copy of \underline{X} for current permutation
- 5: **for** $j \in \pi_{\mathcal{J}}$ **do**
- 6: **if** $\mathcal{K}_t^{0\pi} = \emptyset$ **then**
- 7: **break** ▷ If all targets are observed, no more allocations are necessary
- 8: **end if**
- 9: $i^* \leftarrow$ eqn. (35)
- 10: $\underline{X}_{i^*j^*t}^{\pi} \leftarrow 1$
- 11: **for** $k = 1, \dots, q$ **do**
- 12: **if** $M_{i^*j^*t k}^b = 1$ **then**
- 13: $\mathcal{K}_t^{0\pi} \leftarrow \mathcal{K}_t^0 \setminus \{k \mid M_{i^*j^*t k}^b = 1\}$ ▷ Remove newly targets observed from set of unobserved targets
- 14: **end if**
- 15: **end for**
- 16: **end for**
- 17: $\Delta^{\pi} \leftarrow |\mathcal{K}_t^0| - |\mathcal{K}_t^{0\pi}|$ ▷ Number of additional targets observed by current permutation
- 18: **end for**
- 19: $\pi^* \leftarrow \min_{\pi} \Delta^{\pi}$ ▷ Choose allocation best permutation
- 20: $\underline{X} \leftarrow \underline{X}^{\pi^*}$ ▷ Take \underline{X} corresponding to best permutation
- 21: **return** \underline{X}

C. Heuristics for Neighborhood Facility Swap

The major limitation of the LR procedure is the lack of convergence guarantee; depending on, among other things, the choice of constraints that are relaxed and the construction of the heuristic lower bound solution, it is possible that the procedure is no longer able to reduce the optimality gap. For the problem in question, preliminary experiments with the greedy/full-factorial allocation heuristics alone have revealed that while the algorithm performs well in most cases, there are instances where it gets stuck with intuitively suboptimal choice of observer locations. We thus develop additional heuristics to mutate the

Consider a list of sets C of length n , where each entry is a set of neighboring facility indices to each corresponding facility j . For a given facility j , we denote with ξ_1, \dots, ξ_{w_j} its w_j neighboring facilities; then, we may express C_j as

$$C_j = \{\text{neighboring facility indices of } j\} = \{\xi_1, \dots, \xi_{w_j} \mid \xi \in \text{Neighborhood}(j)\} \quad (36)$$

where $\text{Neighborhood}(j)$ is a set of slot indices that are in the “neighborhood” of slot j . We conceive two kinds of “neighborhoods”, one within the same LPO as j but with shifted phasing, and another with similar phasing but on different LPOs. These are defined in further details in the subsequent subsections.

Using C_j , the neighborhood swap heuristic which seeks to improve an existing solution by exploring neighboring candidate facility slots is conceived. This involves creating a new decision vector Y_{new} by mutating one of the active slot in the existing best feasible Y_{best} , denoted as j_{out} , to one of its neighboring slot in $C_{j_{\text{out}}}$, and evaluating the resulting feasible allocations X_{new} and θ_{new} using the heuristic feasible allocation algorithm 1. This is repeated for each candidate neighboring slots C_j of each active slot in Y_{best} . This procedure is summarized in Algorithm 4.

Algorithm 4 Neighborhood Swap

Require: $C_j, X_{\text{best}}, Y_{\text{best}}, Z_{\text{best}}, \theta_{\text{best}}$

- 1: $\mathcal{J}^Y \leftarrow \{j \in 1, \dots, n \mid Y_{\text{best},j} = 1\}$
- 2: **for** $j_{\text{out}} \in \mathcal{J}^Y$ **do**
- 3: **for** $j_{\text{in}} \in C_{j_{\text{out}}}$ **do**
- 4: $\mathcal{J}^{Y_{\text{new}}} \leftarrow \mathcal{J}^Y \cup \{j_{\text{in}}\} \setminus j_{\text{out}}$ ▷ Create new set of facilities by removing j_{out} and adding j_{in}
- 5: $Y_{\text{new}} \leftarrow \text{SetToVector}(\mathcal{J}^{Y_{\text{new}}})$ ▷ Convert set to vector
- 6: $X_{\text{new}}, \theta_{\text{new}} \leftarrow \text{HeuristicFeasibleAllocation}(Y_{\text{new}})$ ▷ Heuristically compute feasible allocation
- 7: $Z_{\text{new}} \leftarrow \text{eqn. (15a)}$ ▷ Evaluate objective
- 8: **if** $Z_{\text{new}} > Z_{\text{best}}$ **then** ▷ If swap results in improvement, overwrite best solution
- 9: $X_{\text{best}} \leftarrow X_{\text{new}}$
- 10: $Y_{\text{best}} \leftarrow Y_{\text{new}}$
- 11: $Z_{\text{best}} \leftarrow Z_{\text{new}}$
- 12: $\theta_{\text{best}} \leftarrow \theta_{\text{new}}$
- 13: **end if**
- 14: **end for**
- 15: **end for**
- 16: **return** $X_{\text{best}}, Y_{\text{best}}, Z_{\text{best}}, \theta_{\text{best}}$

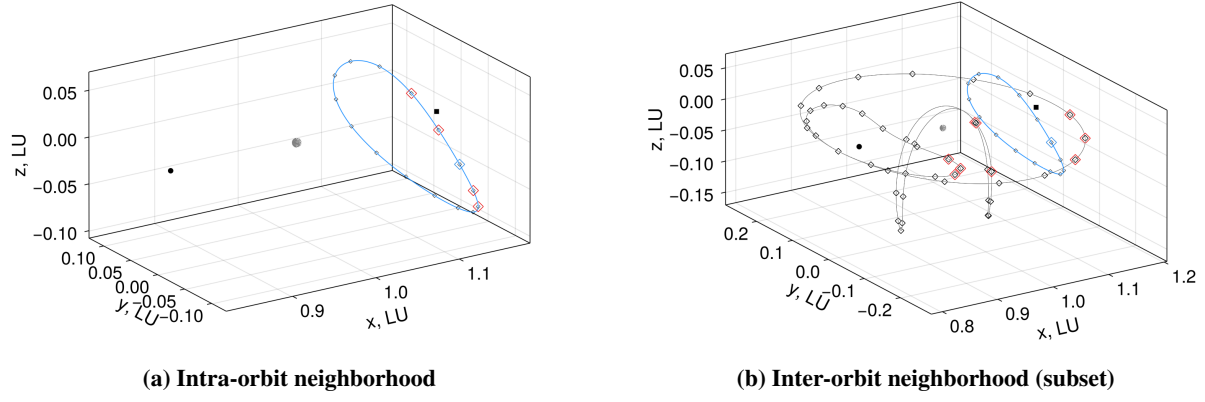


Fig. 9 Example of (a) intra-orbit and (b) inter-orbit neighborhood, shown for a 2:1 resonant L2 Southern Halo Orbit

1. Intra-Orbit Neighborhood

The intra-orbit neighborhood is defined based on proximity in angular location along a given LPO. Specifically, let $\Xi_j^\alpha \subset \mathcal{J}$ denote all other facility indices that are on the same LPO as j ; for a given j , its LPO is discretized into b_j slots according to equation (3), then Ξ_j^α has $b_j - 1$ elements, excluding j itself. We further define $\Delta\varphi_{j\xi}$ as the angular separation between facility locations j and $\xi \in \Xi_j^\alpha$. Then, we define the permutation of ξ , denoted by π_{C^α} , for which the absolute value of $\Delta\varphi_{j\xi}$ is in ascending order,

$$|\Delta\varphi_{j\pi_{C^\alpha}(1)}| \leq |\Delta\varphi_{j\pi_{C^\alpha}(2)}| \leq \dots \leq |\Delta\varphi_{j\pi_{C^\alpha}(b_j-1)}| \quad (37)$$

to arrive at the intra-orbit neighborhood C_j^α of size $c^\alpha \leq b_j - 1$, given by

$$C_j^\alpha = \{\xi_\kappa \mid \kappa = \pi_{C^\alpha}(1), \dots, \pi_{C^\alpha}(c^\alpha)\} \quad (38)$$

Note that c^α is a tuning parameter for the heuristics that dictates the angular separation to be considered for swapping; while a larger c^α results in a more thorough evaluation of the neighborhood, the size of C_j^α directly impacts the number of iterations of the inner for-loop in algorithm 4, and must thus be kept reasonably low. It is also recommended to choose c^α as a multiple of 2 to evenly explore candidate locations ξ that either lead or lag in angular location relative to the originally chosen j .

2. Inter-Orbit Neighborhood

The inter-orbit neighborhood of j is defined as the set of candidate facility locations that are (1) on different LPOs with the same $M:N$ resonance, and (2) exhibit a similar solar phase angle ϕ_S with respect to a reference target at a reference epoch. The latter condition is required to isolate a single slot from the slots along an LPO with the same

resonance as the LPO along which slot j is located.

To arrive at an expression for the inter-orbit neighborhood of j , we begin by defining by \mathcal{P}_j the set of LPOs that have the same $M:N$ resonance as the LPO of j . Then, for each candidate facility location ξ along each LPO $\rho \in \mathcal{P}_j$, we determine the slot ξ_ρ^* that has the smallest angular separation with respect to a reference target at position $\bar{\mathbf{r}}_k$ and for a given the line-of-sight vector from the Sun to target k , \mathbf{l}_{Sk} ,

$$\xi_\rho^* = \underset{\xi}{\operatorname{argmin}} \left(\mathbf{l}_{jk}^T \mathbf{l}_{Sk} - \mathbf{l}_{\xi k}^T \mathbf{l}_{Sk} \right) \quad (39)$$

Note that the choice of \mathbf{l}_{Sk} is a direct consequence of choosing a reference epoch. In this work, we choose the initial epoch with Earth-Moon-Sun alignment as the reference, and define the reference target position as the weighted sum of all considered targets across all times,

$$\bar{\mathbf{r}}_k = \frac{1}{\ell q} \sum_{t=1}^{\ell} \sum_{k=1}^q \mathbf{r}_k(t) \quad (40)$$

Finally, the inter-orbit neighborhood C_j is given by

$$C_j = \{ \xi_\rho^* \mid \forall \rho \in \mathcal{P}_j \} \quad (41)$$

Note that the inter-orbit neighborhood swap is only attempted if the LR and the corresponding feasible solution from algorithm 1 fail to reduce the optimality gap over a pre-defined number of iterations; this is due to the computational expense of this swap approach, requiring to run algorithm 1 for each candidate solution, as well as to avoid prematurely swapping to different LPO slots before the nearby slots in phase along a given LPO has been sufficiently explored.

D. Subgradient Optimization

For the dual problem, we seek to obtain multipliers λ_{jt} and η_{tk} that yields the tightest upper bound,

$$Z_{\text{LR}}^* = \min_{\lambda_{jt}, \eta_{tk}} Z_{\text{LR}} \quad (42)$$

The Lagrange multipliers are updated using the subgradient method

$$\lambda_{jt}^{(h+1)} = \lambda_{jt}^{(h)} + s^{(h)} \left(\sum_{i=1}^m M_{ijtk} \bar{X}_{ijt} - 1 \right) \quad \forall j, t \quad (43)$$

$$\eta_{tk}^{(h+1)} = \lambda_{jt}^{(h)} + s^{(h)} \left(\bar{\theta}_{tk} - \sum_{i=1}^m \sum_{j=1}^n M_{ijtk} \bar{X}_{ijt} \right) \quad \forall t, k \quad (44)$$

where $s^{(h)}$ is the step-size given by

$$s^{(h)} = \frac{\mu^{(h)}(Z_{\text{LR}} - Z_{\text{LH}})}{\left[\sum_{j=1}^n \sum_{t=1}^{\ell} \max(0, \sum_{i=1}^m M_{ijtk} \bar{X}_{ijt} - 1) \right]^2 \left[\sum_{t=1}^{\ell} \sum_{k=1}^q \max(0, \bar{\theta}_{tk} - \sum_{i=1}^m \sum_{j=1}^n M_{ijtk} \bar{X}_{ijt}) \right]^2} \quad (45)$$

In equation (45), $\mu^{(h)}$ is a hyperparameter for scaling the step-size, which is reduced if no reduction of the gap between the lower-bound and upper-bound solutions is observed; initially, $\mu^{(0)} = 2.0$ is typically chosen when employing the subgradient update, with a step reduction factor of 0.5.

E. Implementation Considerations

The LM is implemented using the Julia language. We make note of three particular design choices that are made to improve the performance of the algorithm, namely on the initialization of the Lagrange multipliers, parallelism and function memorization.

1. Initialization of Lagrange Multipliers

The choice of the initial values of the Lagrange multipliers requires some care, as the LM does not have a guarantee of convergence. One approach commonly adopted is to initialize them using the dual of the corresponding constraints for the linear program (LP)-relaxed problem, but our initial investigation has shown that this does not yield a particular advantage, despite the additional cost of having to solve the relaxed problem.

2. Parallelism

For a given choice of facilities Y , the feasible allocation construction algorithm 1 makes allocation decisions X_{ijt} for each time step, each of which is independent of allocation decisions at other time steps. This makes the algorithm well-suited for parallelism; we opt for the multiple-threading paradigm through Julia's `Threads` `@threads` decorator to the for-loop in line 3 through 20, as the operation within each loop is not too expensive, and we gain more benefit from a shared memory. Note that both the intra- and inter-orbit neighborhood swap schemes require recomputing the best heuristic allocations X_{ijt} for each new hypothesized Y , thus a speed-up of algorithm 1 is particularly beneficial to speed up the overall Lagrangean method.

3. Memoization

During the heuristic process of the Lagrangean method, it is possible that the Lagrangean relaxed solution \bar{Y} or the result of either an intra- and inter-orbit neighborhood swap result in a choice of facilities that has already been considered by the algorithm. We make use of function memoization on the feasible allocation construction algorithm 1 by storing the outputs \underline{X} and $\underline{\theta}$ that results from a given set of active facility indices $\mathcal{J}^{\bar{Y}}$.

Table 2 Problem dimensions for each demand and observer parameters

Demand	SOI	Cone of shame	LET transit
Number of pointing directions m	14	14	14
Number of facility locations n	1212	1212	1212
Number of time steps ℓ	120	120	120
Number of targets q	120	304	675
Fraction of entries in M^b	$\bar{m}_{\text{crit}} = 15$	0.0111	0.0047
	$\bar{m}_{\text{crit}} = 18$	0.0496	0.0460
	$\bar{m}_{\text{crit}} = 20$	0.0572	0.0581
FOV = 120°	$\bar{m}_{\text{crit}} = 15$	0.0421	0.0180
	$\bar{m}_{\text{crit}} = 18$	0.1881	0.1711
	$\bar{m}_{\text{crit}} = 20$	0.2198	0.2177

VI. Numerical Results

The TE- p -MP is solved for various choices of observation demand as well as observer parameters. Each instance is solved using the LM and Gurobi, in order to study the efficacy of the proposed former approach. This Section initially focuses on comparing the performance of the two methods, emphasizing on the quality of solutions they yield. Then, closer attention is drawn to the obtained architectures for a select number of instances, in order to provide insights on the CSSA problem.

The three sets of demand presented in Section III are considered; the corresponding problem dimensions are summarized in Table 2. For each set of demand introduced in Section III, we consider LPOs given in Table 8, with an approximate time-spacing parameter $\Delta t_b = 12$ hours. Using equation (3), this results in $n = 1212$ candidate facility slots in total, summarized in Table 8. For the system with all observers to return to their original position, the considered set of resonances requires 4 synodic months. A time-step of 60 steps per synodic month, corresponding to roughly 24 hours, is selected, thus resulting in $\ell = 120$ time-steps. All problem instances are solved on a desktop PC running on eight i7-10700 CPU cores at 2.90GHz. Table 3 gives the hyperparameters for the LM; Table 4 gives the non-default options set with Gurobi version 9.5.0.

A. Comparison of Lagrangean Method against Gurobi

We first compare the proposed Lagrangean method against Gurobi, for TE- p -MP instances with static and dynamic demands. For the sake of a fair comparison, we set a time limit of 500 seconds on both approaches to assess their performance. In addition, the solution obtained by running Gurobi with a time limit of 3600 seconds is reported. Note that while extending the time limit may allow Gurobi to find better solutions, this is not necessarily desirable, especially when various problem parameters, such as the number of satellites p , cut of magnitude, or FOV, must be explored and optimized. Nevertheless, the solution from Gurobi with a 3600 seconds time limit serves as a proxy of a near-optimal

solution obtained with a *reasonably* long time limit in most instances.

Tables 5, 6, and 7 report the sum of targets observed across all time steps, Θ , and the actual CPU solve time for each of the three observation demands, respectively. In all three cases, the solutions obtained with Gurobi using time limits of 500 and 3600 seconds and with the LM using a time limit of 500 seconds are reported. In addition, the percentage difference of the Lagrangean method solution with respect to each Gurobi solution is reported. Note that the actual CPU solve time may exceed 500 seconds for both Gurobi and the Lagrangean method; in Gurobi, this is due to the computation of attributes associated with the terminated solution, while with the Lagrangean method, the solve time is checked between the generation of feasible lower bound solution, which may start before the solve time limit, but exceed it before another solve time check happens.

Across the three demands, we first note that LM finds a superior solution to Gurobi with the 500 seconds time limit (i.e., under a fair condition) in all cases with $\bar{m}_{\text{crit}} = 20$, and in all except two cases with $\bar{m}_{\text{crit}} = 18$, the latter of which corresponding to $p = 2$ with the Cone of Shame and LET demands. For cases with $\bar{m}_{\text{crit}} = 15$, Gurobi finds competitive solutions for the SOI and Cone of Shame demands, while it is found to struggle with the LET demand for $p \geq 3$. Letting Gurobi run for up to 3600 seconds improves the solution in some instances, but the behavior is hard to predict. For example, in the SOI demand, cases with $\bar{m}_{\text{crit}} = 18$ and $p = 3$ has a solution that improves from $\Theta_{500} = 0.2802$ to $\Theta_{3600} = 0.9885$, while with $\bar{m}_{\text{crit}} = 18$ and $p = 4$, the solution remains at $\Theta_{500} = \Theta_{3600} = 0.2863$. The performance of Gurobi is largely dictated by how effective the underlying B&B algorithm can prune the nodes as well as the presolve algorithm, both of which are in turn impacted by the solver's hyperparameters.

The performance of Gurobi, both after 500 and 3600 seconds, may thus be seen as a measure of the difficulty of the TE- p -MP instance; the problem appears to be easy when the *observation* is difficult, with observers are few (low p) and/or are equipped with worse sensors (lower \bar{m}_{crit}), or when the observation is easy, with many observers (high p) and/or high-performance sensors (higher \bar{m}_{crit}), resulting in an instance where the observation task is “easy”. Examples of the former include the cases with $\bar{m}_{\text{crit}} = 15, 18$ and $p = 2, 3$ for the LET demand, while examples of the latter include the cases with $\bar{m}_{\text{crit}} = 15$ and $p = 4, 5$, also for the LET demand. Instances of intermediate observation difficulty, such as the cases with $\bar{m}_{\text{crit}} = 18, 20$ and $p = 2 \sim 5$ for the Cone of Shame demand, are found to result in the poorest performances from Gurobi.

In contrast, the performance of the LM is found to be consistent in terms of observation condition: increasing p always increases Θ_{LH} , while increasing \bar{m}_{crit} also increases Θ_{LH} except for the two cases with the Cone of Shame demand with $p = 2, 3$ going from $\bar{m}_{\text{crit}} = 18$ to 20, albeit with a small reduction, from 0.7334 to 0.7297 with $p = 2$, and from 0.8192 to 0.8080 with $p = 3$. Note that these two instances correspond to some of the cases where Gurobi struggles the most. Among the 36 instances, 11 instances resulted in an LM solution that was inferior to Gurobi after 500 seconds; within them, only 4 cases resulted in a solution that was worse by over 10%. Overall, the consistency of the LM offers an attractive reliable approach for assessing the achievable observation from a given TE- p -MP instance.

Table 3 Lagrangean method hyperparameters

Option	Value
Max number of iterations	30
Gap tolerance	0.01
Max number of iterations without improvements	10
Number of iterations with no improvement to reduce step-size parameter $\mu^{(h)}$	5
Number of slots considered for intra-orbit neighborhood swap	4
Number of iterations with no improvement to try inter-orbit neighborhood swap	4
Relocation strategy	FullFactorialGreedy

Table 4 Non-default Gurobi options

Option	Value
Gap tolerance	0.01
Method	2
MIPFocus	2

Alternatively, one may consider using Gurobi with a relatively short solve time limit such as 500 seconds, and use the LM as a consistent fallback solver to recover descent solutions in case Gurobi under-performs.

B. Analysis of CSSA Coverage

As a demonstration of the usability of the proposed problem formulation and the LM, we now look in detail at the trade space for designing CSSA constellations for the SOI, cone of shame, and LET transit window demands. For consistency across all cases, all results are based on solutions obtained using the LM, with a time limit of 1000 seconds. We provide insight on a select number of architectures across a few combinations of parameters. The full list of LPOs used by each problem from Gurobi and LM are provided in Tables in Appendix VII.B.

1. Sphere of Influence

Competitive solutions with the SOI demand are found to utilize planar LPOs, particularly the 1:1 resonant L1 and L2 Lyapunov orbits, and DROs of various resonances. We particularly focus on two types of solutions: the former is an example using the Lyapunov orbits, with $\bar{m}_{\text{crit}} = 20$ and $p = 2$, and the latter is an example using the DROs, with $\bar{m}_{\text{crit}} = 20$ and $p = 5$, shown in Figure 10.

The Lyapunov orbit-based constellation in Figure 10a contains two observers on the 1:1 resonant L1 Lyapunov, which extend beyond the region spanned by the SOI along the y-axis in the Earth-Moon rotating frame. Clock-wise rotating LPOs with 1:1 resonance are particularly well suited for optical observations since the solar phase angle ϕ_S in the direction of a static target remains nearly constant [2, 13]; while the 1:1 L1 Lyapunov has a varying distance from the set of targets, choosing the appropriate phase along the LPO provides consistently low \bar{m}_{target} , as \bar{m}_{target} has a

Table 5 TE- p -MP instance with SOI demand and for $\text{FOV} = 60^\circ$ solved using Gurobi (MIPGap 1%) versus Lagrangean method. All reported times are in seconds.

(a) $\bar{m}_{\text{crit}} = 15$										
p	Gurobi (TimeLimit = 500)			Gurobi (TimeLimit = 3600)			Lagrangean Method			
	Θ_{500}	Time	Status	Θ_{3600}	Time	Status	Θ_{LH}	Time	% diff. to Θ_{500}	% diff. to Θ_{3600}
2	0.1558	316	OPTIMAL	-	-	-	0.1506	507	-3.34	-3.34
3	0.2238	500	TIME_LIMIT	0.2238	3600	TIME_LIMIT	0.2057	553	-8.10	-8.10
4	0.2653	500	TIME_LIMIT	0.2741	3601	TIME_LIMIT	0.2600	543	-2.02	-5.14
5	0.3131	500	TIME_LIMIT	0.3135	3600	TIME_LIMIT	0.3104	551	-0.86	-1.00

(b) $\bar{m}_{\text{crit}} = 18$										
p	Gurobi (TimeLimit = 500)			Gurobi (TimeLimit = 3600)			Lagrangean Method			
	Θ_{500}	Time	Status	Θ_{3600}	Time	Status	Θ_{LH}	Time	% diff. to Θ_{500}	% diff. to Θ_{3600}
2	0.8567	503	TIME_LIMIT	0.9160	3601	TIME_LIMIT	0.5506	503	-35.72	-39.89
3	0.2802	500	TIME_LIMIT	0.9885	3600	TIME_LIMIT	0.7007	515	+150.06	-29.11
4	0.2863	500	TIME_LIMIT	0.2863	3600	TIME_LIMIT	0.7858	534	+174.46	+174.46
5	0.3665	500	TIME_LIMIT	0.3665	3600	TIME_LIMIT	0.9383	534	+156.04	+156.04

(c) $\bar{m}_{\text{crit}} = 20$										
p	Gurobi (TimeLimit = 500)			Gurobi (TimeLimit = 3600)			Lagrangean Method			
	Θ_{500}	Time	Status	Θ_{3600}	Time	Status	Θ_{LH}	Time	% diff. to Θ_{500}	% diff. to Θ_{3600}
2	0.4176	503	TIME_LIMIT	0.9367	3721	TIME_LIMIT	0.5791	573	+38.66	-38.18
3	0.4383	504	TIME_LIMIT	0.9662	3603	TIME_LIMIT	0.6514	564	+48.61	-32.58
4	0.4690	500	TIME_LIMIT	0.9173	3601	TIME_LIMIT	0.7949	533	+69.47	-13.35
5	0.5332	500	TIME_LIMIT	0.9926	1633	OPTIMAL	0.8743	588	+63.97	-11.92

stronger dependence on ϕ_S over the distance, as shown in Figure 5. Meanwhile, the two L2 Lyapunov orbits are placed with some along-track separation, but not at 180° apart from one another; this is a manifestation of the property of the clock-wise rotating 1:1 resonant LPO, where both observers are preferentially placed in angular locations that provide sufficiently good illumination conditions.

This is contrasted by the latter solution shown in Figure 10b, where five observers are all placed in a 3:2 resonant DRO, with equal angular separation. Because the resonance is not 1:1, angular locations along the LPO with good or poor illumination conditions vary over time. Thus, the five observers are used in a complementary manner, in such a way that there are always at least two to three observers that can monitor the set of targets.

2. Cone of Shame

In the Cone of Shame demand, the 1:1 resonant L1 Lyapunov orbit is found to be used in many competitive instances. Figure 11 shows the LM-based solutions for $p = 3, 4, 5$ and $\bar{m}_{\text{crit}} = 20$. In these three solutions, as the number of observers p is increased, an additional observer is added to the same orbit, resulting in an increase in coverage fraction

Table 6 TE- p -MP instance with Cone of Shame demand and FOV = 60° solved using Gurobi (MIPGap 1%) versus Lagrangean method. All reported times are in seconds.

(a) $\bar{m}_{\text{crit}} = 15$											
p	Gurobi (TimeLimit = 500)			Gurobi (TimeLimit = 3600)			Lagrangean Method				
	Θ_{500}	Time	Status	Θ_{3600}	Time	Status	Θ_{LH}	Time	% diff. to Θ_{500}	% diff. to Θ_{3600}	
2	0.1061	89	OPTIMAL	-	-	-	0.1033	540	-2.68	-2.68	
3	0.1540	500	TIME_LIMIT	0.1540	3522	OPTIMAL	0.1318	520	-14.39	-14.39	
4	0.1999	500	TIME_LIMIT	0.1999	3603	TIME_LIMIT	0.1837	504	-8.09	-8.09	
5	0.2435	502	TIME_LIMIT	0.2435	3600	TIME_LIMIT	0.2176	535	-10.61	-10.61	

(b) $\bar{m}_{\text{crit}} = 18$											
p	Gurobi (TimeLimit = 500)			Gurobi (TimeLimit = 3600)			Lagrangean Method				
	Θ_{500}	Time	Status	Θ_{3600}	Time	Status	Θ_{LH}	Time	% diff. to Θ_{500}	% diff. to Θ_{3600}	
2	0.1098	501	TIME_LIMIT	0.7259	3607	TIME_LIMIT	0.6194	530	+463.94	-14.67	
3	0.1358	501	TIME_LIMIT	0.8315	3601	TIME_LIMIT	0.7334	526	+439.96	-11.80	
4	0.1439	500	TIME_LIMIT	0.6670	3601	TIME_LIMIT	0.8192	513	+469.09	+22.81	
5	0.1669	500	TIME_LIMIT	0.7498	3603	TIME_LIMIT	0.8454	559	+406.39	+12.75	

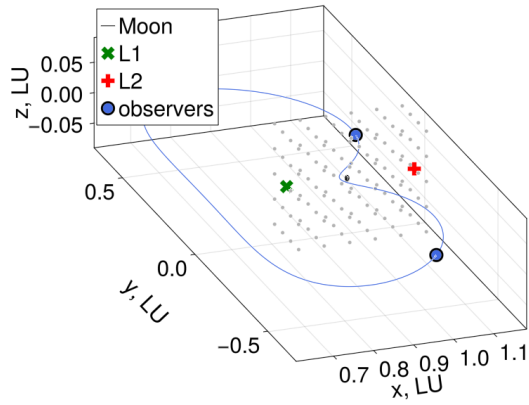
(c) $\bar{m}_{\text{crit}} = 20$											
p	Gurobi (TimeLimit = 500)			Gurobi (TimeLimit = 3600)			Lagrangean Method				
	Θ_{500}	Time	Status	Θ_{3600}	Time	Status	Θ_{LH}	Time	% diff. to Θ_{500}	% diff. to Θ_{3600}	
2	0.1321	506	TIME_LIMIT	0.1321	3611	TIME_LIMIT	0.6934	532	+424.92	+424.92	
3	0.1612	506	TIME_LIMIT	0.1612	3606	TIME_LIMIT	0.7297	529	+352.76	+352.76	
4	0.1925	505	TIME_LIMIT	0.1925	3613	TIME_LIMIT	0.8080	517	+319.81	+319.81	
5	0.2140	506	TIME_LIMIT	0.2140	3613	TIME_LIMIT	0.9322	511	+335.53	+335.53	

as well. As it was noted from the solution in Figure 10a, the clock-wise rotating 1:1 resonant LPOs are placed in a leading/trailing configuration along the LPO rather than being placed at equal anomaly separation. The persistence of this train-like configuration across multiple problem instances highlights the efficacy of this constellation design strategy, particularly for monitoring targets in the Cone of Shame.

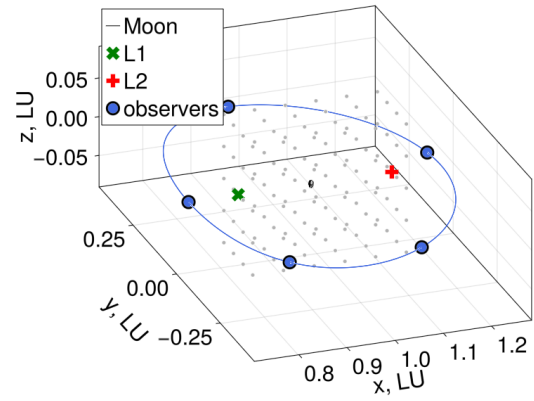
3. Low-Energy Transfer Transit Window

We finally look into solutions for the LET transit demand. We first compare solutions with increasing cut-off magnitude from 15 to 20, with observers fixed to $p = 4$; the corresponding architectures, obtained by the LM, are shown in Figures 12a, 12b, and 12c. When the cut-off magnitude is lower, targets become harder to observe, and the observers are placed in a 2:1 resonant L2 Halo orbit that is closer to the set of targets; this comes with the disadvantage that the observer is able to fit fewer targets within its FOV at a given time. Meanwhile, the solutions at $\bar{m}_{\text{crit}} = 18, 20$ use a 3:1 resonant L2 Halo orbit that is further away, offering larger coverage from a single sensor pointing allocation.

We also recognize that the train-like constellation, reminiscent of solutions from Figures 10a or 11, is used on the 2:1

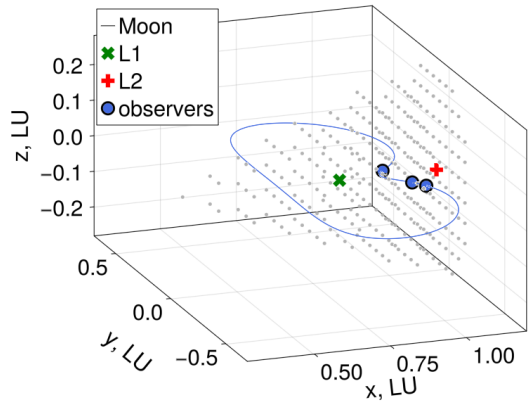


(a) Gurobi solution with $\bar{m}_{\text{crit}} = 20, p = 2$

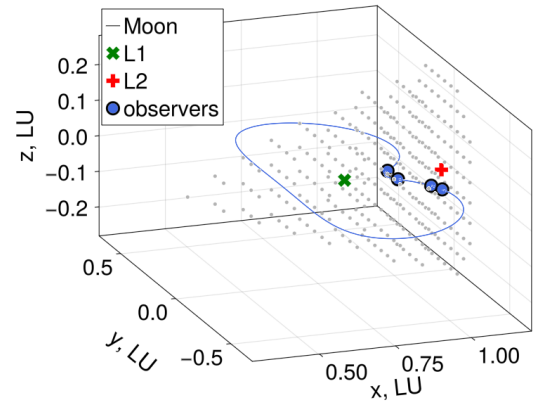


(b) Gurobi solution with $\bar{m}_{\text{crit}} = 20, p = 5$

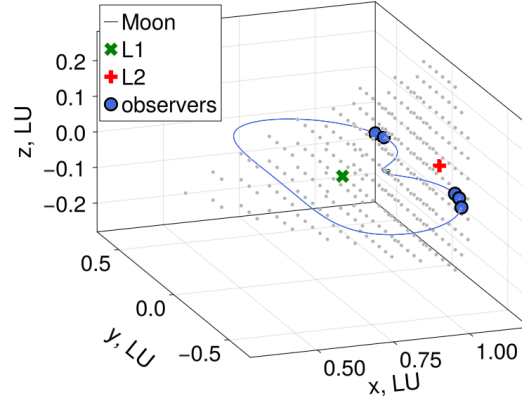
Fig. 10 Select architecture solutions for Sphere of Influence demand at time-step $t = 1$



(a) Lagrangean method solution with $\bar{m}_{\text{crit}} = 20, p = 3$



(b) Lagrangean method solution with $\bar{m}_{\text{crit}} = 20, p = 4$



(c) Lagrangean method solution with $\bar{m}_{\text{crit}} = 20, p = 5$

Fig. 11 Select architecture solutions for Cone of Shame demand at time-step $t = 1$

Table 7 TE- p -MP instance with LET demand and FOV = 60° solved using Gurobi (MIPGap 1%) versus Lagrangean method. All reported times are in seconds.

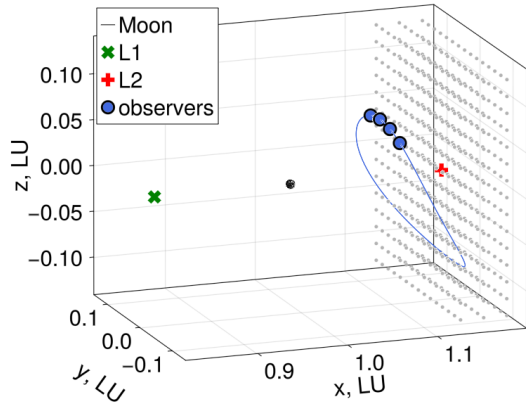
(a) $\bar{m}_{\text{crit}} = 15$											
p	Gurobi (TimeLimit = 500)			Gurobi (TimeLimit = 3600)			Lagrangean Method				
	Θ_{500}	Time	Status	Θ_{3600}	Time	Status	Θ_{LH}	Time	% diff. to Θ_{500}	% diff. to Θ_{3600}	
2	0.3737	39	OPTIMAL	-	-	-	0.3144	534	-15.86	-15.86	
3	0.2406	500	TIME_LIMIT	0.5078	1291	OPTIMAL	0.3967	529	+64.89	-21.88	
4	0.1703	500	TIME_LIMIT	0.5959	3508	OPTIMAL	0.4681	533	+174.92	-21.45	
5	0.1840	500	TIME_LIMIT	0.6674	3600	TIME_LIMIT	0.5502	545	+199.05	-17.56	

(b) $\bar{m}_{\text{crit}} = 18$											
p	Gurobi (TimeLimit = 500)			Gurobi (TimeLimit = 3600)			Lagrangean Method				
	Θ_{500}	Time	Status	Θ_{3600}	Time	Status	Θ_{LH}	Time	% diff. to Θ_{500}	% diff. to Θ_{3600}	
2	0.9212	500	TIME_LIMIT	0.9398	3600	TIME_LIMIT	0.8353	524	-9.33	-11.12	
3	0.4414	500	TIME_LIMIT	0.9546	3650	TIME_LIMIT	0.9056	517	+105.16	-5.14	
4	0.4582	500	TIME_LIMIT	0.4582	3600	TIME_LIMIT	0.9423	586	+105.64	+105.64	
5	0.5335	501	TIME_LIMIT	0.9921	2220	OPTIMAL	0.9545	500	+78.89	-3.79	

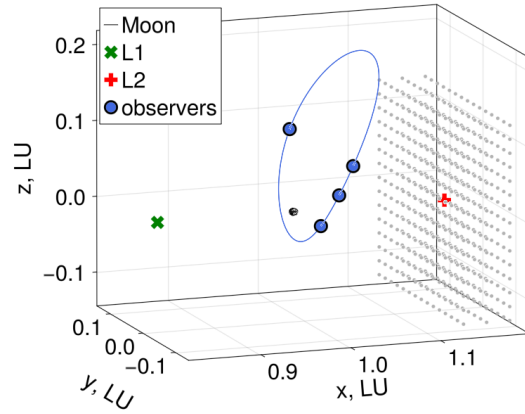
(c) $\bar{m}_{\text{crit}} = 20$											
p	Gurobi (TimeLimit = 500)			Gurobi (TimeLimit = 3600)			Lagrangean Method				
	Θ_{500}	Time	Status	Θ_{3600}	Time	Status	Θ_{LH}	Time	% diff. to Θ_{500}	% diff. to Θ_{3600}	
2	0.4607	500	TIME_LIMIT	0.9701	3600	TIME_LIMIT	0.8807	615	+91.17	-9.22	
3	0.5431	502	TIME_LIMIT	0.5431	3600	TIME_LIMIT	0.9461	512	+74.21	+74.21	
4	0.0000	500	TIME_LIMIT	0.9937	723	OPTIMAL	0.9868	621	+Inf	-0.69	
5	0.0000	502	TIME_LIMIT	0.9958	1327	OPTIMAL	0.9774	538	+Inf	-1.85	

resonant Halo for $\bar{m}_{\text{crit}} = 15$, and for three of the four observers on the 3:1 resonant Halo for $\bar{m}_{\text{crit}} = 18, 20$. The fourth observer in the last two cases is placed with a significant angular separation along the LPO to complement the coverage; note that because the LPO is not planar, the illumination conditions are not necessarily poor for this last observer during the times along the LPO where there is a non-negligible out-of-plane component.

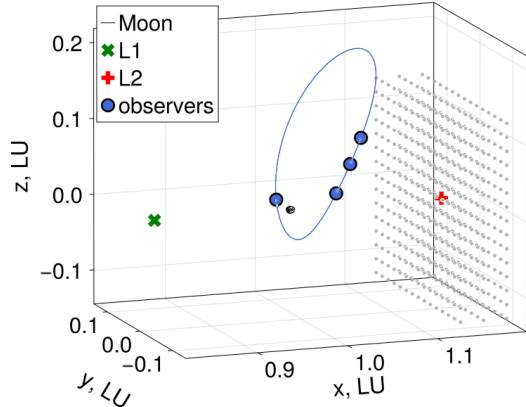
As the observer is increased to $p = 5$, the architecture consists of four 3:1 L2 Halo observers and an additional observer on the 1:1 L1 Lyapunov, as shown in Figure 12d. Now, all four observers on the 3:1 L2 Halo form a train-like configuration, all in adjacent angular locations, and a complementing observer is now placed on a different LPO altogether. Note that the 1:1 resonant L1 Lyapunov is a favorable LPO for placing a single additional observer due to the invariance of the illumination condition; while the larger orbit results in an increased distance from the target set, this does not constitute a penalty in this configuration, where \bar{m}_{crit} is set high.



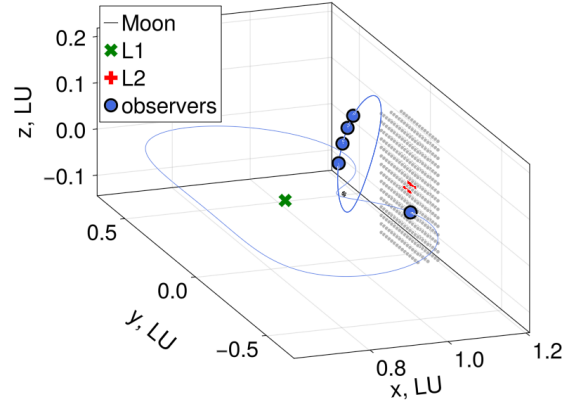
(a) Lagrangean method solution with $\bar{m}_{\text{crit}} = 15$, $p = 4$



(b) Lagrangean method solution with $\bar{m}_{\text{crit}} = 18$, $p = 4$



(c) Lagrangean method solution with $\bar{m}_{\text{crit}} = 20$, $p = 4$



(d) Gurobi solution with $\bar{m}_{\text{crit}} = 20$, $p = 5$

Fig. 12 Select architecture solutions for LET transit demand at time-step $t = 1$

VII. Conclusions

In this work, the TE- p -MP has been formulated to design satellite constellations for CSSA. The problem consists of determining the p optimal observer locations along with the orientation of their optical sensors over time to observe a given set of static or dynamic targets. The resulting optimization problem is a binary linear program (BLP), which is discretized in terms of time, candidate locations of observer spacecraft, and sensor pointing directions. A custom LM based on the relaxation of complicating constraints, coupled with custom heuristics leveraging the problem structure as well as the geometry of the candidate facility locations, has been proposed.

The TE- p -MP, along with the LM, has been demonstrated to find near-optimal solutions for various CSSA scenarios, varying in terms of the distribution of demands or observer parameters. The primary benefit of the LM is the reduction in solve time compared to using generic BLP solvers, which enables exploring the trade space of parameters such as the visible magnitude threshold or the temporal and spatial distribution of observation targets. The LM has been demonstrated to perform in a largely consistent manner across most TE- p -MP instances and to deliver competitive near-optimal constellations, whereas Gurobi's performance is found to be far more precarious, depending on the specific parameters of the instance. Several noteworthy constellations tailored to monitoring demands based on the lunar sphere of influence, the Cone of Shame, and a transit window of LETs have been analyzed to demonstrate the proposed approach. One notable remark is on the existence of train-like constellations, where observers are packed in an along-track formation; this type of solution has been found frequently when the observers are located on clockwise-rotating 1:1 resonant LPOs, where the illumination condition is nearly invariant.

Future works include developing a synergistic scheme to use the LM with B&B algorithms, thus combining LM's capability of quickly generating feasible, competitive solutions, with the B&B's guaranteed capability of closing the optimality gap. The objective of the TE- p -MP may also be modified to account for the cost of changing the sensor's pointing direction. Finally, while this work specifically explored the use of the TE- p -MP for CSSA, a similar formulation may be conceivable for other cislunar constellation-based applications, such as the design of Cislunar on-orbit servicing or GNSS constellations.

Appendix

A. Parameters of Synodic-Resonant LPOs

Parameters of the synodic-resonant LPOs considered as candidate locations are given in Table 8. For LPOs with Southern and Northern families, only values for the Southern member is provided; the initial state of the corresponding Northern member is obtained by flipping the sign of x_0 .

Table 8 Parameters of synodic-resonant LPOs

Family	$M:N$	x_0	z_0	\dot{y}_0	Period, TU	Stability	Slots b
DRO	9:2	0.88976967	0	0.47183463	1.47892343	1.00	14
DRO	4:1	0.88060589	0	0.47011146	1.66378885	1.00	15
DRO	3:1	0.85378188	0	0.47696024	2.21838514	1.00	20
DRO	9:4	0.81807765	0	0.50559384	2.95784685	1.00	27
DRO	2:1	0.79946085	0	0.52703349	3.32757771	1.00	30
DRO	3:2	0.73370014	0	0.62889866	4.43677028	1.00	40
DRO	5:2	0.83249233	0	0.49184571	2.66206217	1.00	24
L2 Halo (Southern)	9:2	1.01958272	-0.18036049	-0.09788185	1.47892343	1.00	14
L2 Halo (Southern)	4:1	1.03352559	-0.18903385	-0.12699215	1.66378885	1.00	15
L2 Halo (Southern)	3:1	1.07203837	-0.20182525	-0.18853332	2.21838514	1.00	20
L2 Halo (Southern)	9:4	1.12518004	-0.18195085	-0.22544142	2.95784685	28.78	27
L2 Halo (Southern)	2:1	1.16846916	-0.09994291	-0.19568201	3.32757771	282.87	30
L2 Halo (Southern)	5:2	1.10193101	-0.19829817	-0.21702846	2.66206217	6.93	24
L2 Halo (Northern)	9:2	1.01958272	0.18036049	-0.09788185	1.47892343	1.00	14
L2 Halo (Northern)	4:1	1.03352559	0.18903385	-0.12699215	1.66378885	1.00	15
L2 Halo (Northern)	3:1	1.07203837	0.20182525	-0.18853332	2.21838514	1.00	20
L2 Halo (Northern)	9:4	1.12518004	0.18195085	-0.22544142	2.95784685	28.78	27
L2 Halo (Northern)	2:1	1.16846916	0.09994291	-0.19568201	3.32757771	282.87	30
L2 Halo (Northern)	5:2	1.10193101	0.19829817	-0.21702846	2.66206217	6.93	24
DPO	4:1	1.06189575	0	0.35989734	1.66378885	2.26	15
DPO	3:1	1.06335021	0	0.38222392	2.21838514	10.98	20
DPO	9:4	1.05547996	0	0.45941661	2.95784685	76.76	27
DPO	2:1	1.04880058	0	0.51457559	3.32757771	159.21	30
DPO	3:2	1.02851298	0	0.71048482	4.43677028	587.57	40
DPO	5:2	1.05978399	0	0.42240630	2.66206217	37.71	24
DPO	1:1	1.00515914	0	1.16888350	6.65515541	1399.19	59
L1 Lyapunov	9:4	0.81109465	0	0.26078428	2.95784685	746.89	27
L1 Lyapunov	2:1	0.79987674	0	0.35828602	3.32757771	407.88	30
L1 Lyapunov	3:2	0.76511295	0	0.49115556	4.43677028	133.00	40
L1 Lyapunov	1:1	0.63394833	0	0.79045684	6.65515541	53.98	59
Butterfly (Northern)	9:4	0.94130132	-0.16165899	-0.03565177	2.95784685	5.79	27
Butterfly (Northern)	2:1	0.91204757	-0.14952514	-0.02724245	3.32757771	12.45	30
Butterfly (Northern)	3:2	0.91414032	-0.14492270	-0.11588220	4.43677028	1.00	40
Butterfly (Northern)	1:1	0.99265217	-0.17814460	-0.26312433	6.65515541	1.00	59
Butterfly (Southern)	9:4	0.94130132	0.16165899	-0.03565177	2.95784685	5.79	27
Butterfly (Southern)	2:1	0.91204757	0.14952514	-0.02724245	3.32757771	12.45	30
Butterfly (Southern)	3:2	0.91414032	0.14492270	-0.11588220	4.43677028	1.00	40
Butterfly (Southern)	1:1	0.99265217	0.17814460	-0.26312433	6.65515541	1.00	59
L2 Lyapunov	3:2	1.02557297	0	0.77068285	4.43677028	115.15	40
L2 Lyapunov	1:1	0.99695262	0	1.64068576	6.65515541	49.78	59

Number of slots is based on $\Delta t_b = 12$ hours, resulting in 1212 slots in total.

B. LPOs used in TE- p -MP

Tables 9, 10, and 11 provide a summary of LPOs used by solutions to the TE- p -MP by Gurobi with a time limit of 3600 seconds and the LM with a time limit of 1000 seconds.

Table 9 LPOs used in TE- p -MP instances with SOI demand from Gurobi and Lagrangean method solutions

(a) $p = 2$			(b) $p = 3$		
\bar{m}_{crit}	Gurobi (3600 sec)	Lagrangean Method	\bar{m}_{crit}	Gurobi (3600 sec)	Lagrangean Method
15	DPO (4:1) $\times 2$	DPO (4:1) $\times 2$	15	DPO (4:1) $\times 3$	DPO (4:1) $\times 3$
18	L1 Lyapunov (1:1) $\times 2$	Butterfly-S (1:1) $\times 1$ Butterfly-N (1:1) $\times 1$	18	L1 Lyapunov (1:1) $\times 2$ DPO (1:1) $\times 1$	Butterfly-S (1:1) $\times 3$
20	L1 Lyapunov (1:1) $\times 2$	DRO (9:4) $\times 1$ Butterfly-S (9:4) $\times 1$	20	L1 Lyapunov (1:1) $\times 1$ DRO (3:2) $\times 2$	Butterfly-N (9:4) $\times 2$ Butterfly-S (9:4) $\times 1$

(c) $p = 4$			(d) $p = 5$		
\bar{m}_{crit}	Gurobi (3600 sec)	Lagrangean Method	\bar{m}_{crit}	Gurobi (3600 sec)	Lagrangean Method
15	DPO (4:1) $\times 4$	DPO (4:1) $\times 4$	15	DPO (3:1) $\times 2$ Butterfly-N (2:1) $\times 2$ Butterfly-S (2:1) $\times 1$	DPO (4:1) $\times 4$ DPO (3:1) $\times 1$
18	DRO (5:2) $\times 1$ L1 Lyapunov (1:1) $\times 1$ DPO (1:1) $\times 1$ L1 Lyapunov (2:1) $\times 1$	Butterfly-S (1:1) $\times 2$ Butterfly-N (1:1) $\times 2$	18	DRO (5:2) $\times 1$ L1 Lyapunov (1:1) $\times 1$ DPO (1:1) $\times 1$ Butterfly-S (3:2) $\times 1$ L1 Lyapunov (2:1) $\times 1$	L1 Lyapunov (1:1) $\times 1$ Butterfly-S (1:1) $\times 1$ Butterfly-N (1:1) $\times 3$ L1 Lyapunov (2:1) $\times 1$
20	DRO (3:2) $\times 4$	Butterfly-N (9:4) $\times 2$ DRO (9:4) $\times 1$ Butterfly-S (9:4) $\times 1$	20	DRO (3:2) $\times 5$	L2 Halo (N) (9:2) $\times 1$ Butterfly-N (9:4) $\times 1$ L2 Halo (S) (9:2) $\times 2$ Butterfly-S (9:4) $\times 1$

References

- [1] Frueh, C., Howell, K., Demars, K. J., and Bhaduria, S., “Cislunar Space Situational Awareness,” *31st AAS/AIAA Spaceflight Mechanics Meeting*, 2021.
- [2] Vendl, J. K., and Holzinger, M. J., “Cislunar Periodic Orbit Analysis for Persistent Space Object Detection Capability,” *Journal of Spacecraft and Rockets*, Vol. 58, No. 4, 2021, pp. 1174–1185. <https://doi.org/10.2514/1.A34909>.
- [3] Holzinger, M. J., Chow, C. C., and Garretson, P., “A Primer on Cislunar Space,” Tech. rep., 2021.
- [4] Gordon, N. G., Benchoubane, N., Kurt, G. K., and Falco, G., “On the Role of Communications for Space Domain Awareness,” 2024, pp. 1–12. URL <http://arxiv.org/abs/2406.05582>.

Table 10 LPOs used in TE- p -MP instances with Cone of Shame demand from Gurobi and Lagrangean method solutions

(a) $p = 2$			(b) $p = 3$	
\bar{m}_{crit}	Gurobi (3600 sec)	Lagrangean Method	\bar{m}_{crit}	Gurobi (3600 sec)
15	L2 Halo (N) (9:2) $\times 1$	Butterfly-S (1:1) $\times 1$	15	L2 Halo (N) (9:2) $\times 1$ L2 Halo (S) (9:2) $\times 1$ Butterfly-N (1:1) $\times 1$
18	L1 Lyapunov (1:1) $\times 2$	L1 Lyapunov (1:1) $\times 2$	18	L1 Lyapunov (1:1) $\times 3$ L2 Lyapunov (1:1) $\times 2$
20	DPO (1:1) $\times 1$ L1 Lyapunov (2:1) $\times 1$	L1 Lyapunov (1:1) $\times 2$	20	DRO (5:2) $\times 1$ DPO (1:1) $\times 1$ L1 Lyapunov (2:1) $\times 1$

(c) $p = 4$			(d) $p = 5$	
\bar{m}_{crit}	Gurobi (3600 sec)	Lagrangean Method	\bar{m}_{crit}	Gurobi (3600 sec)
15	Butterfly-S (1:1) $\times 2$ Butterfly-N (1:1) $\times 2$	Butterfly-S (1:1) $\times 2$ Butterfly-N (1:1) $\times 2$	15	L2 Halo (N) (9:2) $\times 1$ Butterfly-S (1:1) $\times 1$ Butterfly-S (3:2) $\times 1$ L2 Halo (S) (9:2) $\times 1$ Butterfly-N (1:1) $\times 1$
18	L1 Lyapunov (1:1) $\times 3$ L2 Lyapunov (1:1) $\times 1$	L1 Lyapunov (1:1) $\times 1$ L2 Lyapunov (1:1) $\times 3$	18	L1 Lyapunov (1:1) $\times 2$ Butterfly-S (1:1) $\times 1$ L2 Lyapunov (1:1) $\times 2$
20	DRO (5:2) $\times 1$ L1 Lyapunov (1:1) $\times 1$ DPO (1:1) $\times 1$ L1 Lyapunov (2:1) $\times 1$	L1 Lyapunov (1:1) $\times 4$	20	DRO (5:2) $\times 1$ L1 Lyapunov (1:1) $\times 1$ DPO (1:1) $\times 1$ Butterfly-S (3:2) $\times 1$ L1 Lyapunov (2:1) $\times 1$

[5] Wilmer, A. P., Bettinger, R. A., Shockley, L. M., and Holzinger, M. J., “Preliminary investigation and proposal of periodic orbits and their utilization for logistics in the cislunar regime,” *Space Policy*, , No. June 2023, 2024, p. 101635. <https://doi.org/10.1016/j.spacepol.2024.101635>, URL <https://doi.org/10.1016/j.spacepol.2024.101635>.

[6] Baker-McEvilly, B., Bhaduria, S., Canales, D., and Frueh, C., “A comprehensive review on Cislunar expansion and space domain awareness,” *Progress in Aerospace Sciences*, Vol. 147, No. June, 2024, p. 101019. <https://doi.org/10.1016/j.paerosci.2024.101019>, URL <https://doi.org/10.1016/j.paerosci.2024.101019>.

[7] Badura, G., Shimane, Y., Gregoire, A., Patel, R., Gilmartin, M., Gangolli, K., Visonneau, L., Tysor, J., Manojkumar, S., Humphrey, F., Valenta, C., Blair, R., Lourenco, N., Hodkin, J., Sudol, A., Borowitz, M., Gunter, B., Christian, J., and Ho, K., “System Design and Analysis for Cislunar Space Domain Awareness Through Distributed Sensors,” *AAS/AIAA Astrodynamics Specialist Conference*, Charlotte, NC, 2022, pp. 1–20.

Table 11 LPOs used in TE- p -MP instances with LET demand from Gurobi and Lagrangean method solutions

(a) $p = 2$			(b) $p = 3$		
\bar{m}_{crit}	Gurobi (3600 sec)	Lagrangean Method	\bar{m}_{crit}	Gurobi (3600 sec)	Lagrangean Method
15	L2 Halo (N) (2:1) $\times 1$ L2 Halo (S) (2:1) $\times 1$	L2 Halo (S) (2:1) $\times 2$	15	L2 Halo (N) (2:1) $\times 1$ L2 Halo (S) (2:1) $\times 2$	L2 Halo (S) (2:1) $\times 3$
18	L1 Lyapunov (1:1) $\times 2$	L2 Halo (N) (3:1) $\times 2$	18	DRO (3:2) $\times 1$ L2 Lyapunov (1:1) $\times 2$	L2 Halo (N) (3:1) $\times 3$
20	L1 Lyapunov (1:1) $\times 2$	L2 Halo (N) (3:1) $\times 2$	20	DRO (5:2) $\times 1$ DPO (1:1) $\times 1$ L1 Lyapunov (2:1) $\times 1$	L2 Halo (N) (3:1) $\times 3$

(c) $p = 4$			(d) $p = 5$		
\bar{m}_{crit}	Gurobi (3600 sec)	Lagrangean Method	\bar{m}_{crit}	Gurobi (3600 sec)	Lagrangean Method
15	L2 Halo (N) (2:1) $\times 2$ L2 Halo (S) (2:1) $\times 2$	L2 Halo (S) (2:1) $\times 4$	15	L2 Halo (N) (2:1) $\times 2$ L2 Halo (S) (2:1) $\times 3$	L2 Halo (N) (2:1) $\times 1$ L2 Halo (S) (2:1) $\times 4$
18	DRO (5:2) $\times 1$ L1 Lyapunov (1:1) $\times 1$ DPO (1:1) $\times 1$ L1 Lyapunov (2:1) $\times 1$	L2 Halo (N) (3:1) $\times 4$	18	DRO (2:1) $\times 1$ DRO (3:2) $\times 4$	L2 Halo (N) (3:1) $\times 5$
20	DRO (3:2) $\times 4$	L2 Halo (N) (3:1) $\times 4$	20	DRO (3:2) $\times 5$	L1 Lyapunov (1:1) $\times 1$ L2 Halo (N) (3:1) $\times 4$

- [8] Bolden, M., Craychee, T., and Griggs, E., “An Evaluation of Observing Constellation Orbit Stability, Low Signal-to-Noise, and the Too-Short-Arc Challenges in the Cislunar Domain,” Maui, Hawai’i., 2020. URL www.amostech.com.
- [9] Cunio, P. M., Bever, M. J., and Flewelling, B. R., “Payload and Constellation Design for a Solar Exclusion-Avoiding Cislunar SSA Fleet,” AMOS, Maui, Hawai’i., 2020. URL www.amostech.com.
- [10] Fahrner, N. O., Correa, J., and Wysack, J., “Capacity-based Cislunar Space Domain Awareness Architecture Optimization Naomi Owens Fahrner Jeremy Correa Joshua Wysack,” *Advanced Maui Optical and Space Surveillance Technologies (AMOS) Conference*, 2022.
- [11] Fedeler, S., Holzinger, M., and Whitacre, W., “Sensor tasking in the cislunar regime using Monte Carlo Tree Search,” *Advances in Space Research*, Vol. 70, No. 3, 2022, pp. 792–811. <https://doi.org/10.1016/j.asr.2022.05.003>.
- [12] Frueh, C., Howell, K., Demars, K. J., Bhaduria, S., and Gupta, M., “Cislunar Space Traffic Management: Surveillance Through Earth-Moon Resonance Orbits,” 2021. URL <http://conference.sdo.esoc.esa.int>.
- [13] Visonneau, L., Shimane, Y., and Ho, K., “Optimizing Multi-Spacecraft Cislunar Space Domain Awareness Systems via Hidden-Genes Genetic Algorithm,” *The Journal of the Astronautical Sciences*, 2023. <https://doi.org/10.1007/s40295-023-00386-8>, URL <http://arxiv.org/abs/2302.09732>.

[14] Dao, P., Haynes, K., Frey, V., Hufford, C., Schindler, K., Payne, T., and Hollon, J., “Simulated Photometry of Objects in Cislunar Orbits,” Maui, Hawai’i, 2020. URL www.amostech.com.

[15] Fowler, E. E., Hurt, S. B., and Paley, D. A., “Orbit Design for Cislunar Space Domain Awareness,” *2nd IAA Conference on Space Situational Awareness (ICSSA)*, 2020.

[16] Thompson, M. R., Ré, N. P., Meek, C., and Cheetham, B., “Cislunar Orbit Determination and Tracking via Simulated Space-Based Measurements,” Maui, Hawai’i, 2021.

[17] Patel, M., Shimane, Y., Lee, H. W., and Ho, K., “Cislunar Satellite Constellation Design via Integer Linear Programming,” *The Journal of the Astronautical Sciences*, Vol. 71, No. 3, 2024, p. 26. <https://doi.org/10.1007/s40295-024-00445-8>, URL <https://doi.org/10.1007/s40295-024-00445-8>.

[18] Wilmer, A. P., and Bettinger, R. A., “Near-Rectilinear Halo Orbit Surveillance using Cislunar Periodic Orbits,” *Advanced Maui Optical and Space Surveillance Technologies (AMOS) Conference*, 2022. URL www.amostech.com.

[19] Wilmer, A. P., Bettinger, R. A., and Little, B. D., “Cislunar Periodic Orbits for Earth–Moon L1 and L2 Lagrange Point Surveillance,” *Journal of Spacecraft and Rockets*, 2022. <https://doi.org/10.2514/1.a35337>.

[20] Dahlke, J. A., Wilmer, A. P., and Bettinger, R. A., “Preliminary Comparative Assessment of L2 and L3 Surveillance Using Select Cislunar Periodic Orbits,” *AAS/AIAA Astrodynamics Specialist Conference*, 2022, pp. 1–19.

[21] Block, J. M., Curtis, D. H., Bettinger, R. A., and Wilmer, A. P., “Cislunar SDA with Low-Fidelity Sensors and Observer Uncertainty Air Force Institute of Technology David H . Curtis , Robert A . Bettinger , and Adam P . Wilmer Air Force Institute of Technology,” *Advanced Maui Optical and Space Surveillance Technologies (AMOS) Conference*, 2022.

[22] Clareson, T. H., Fox, M. C., Amato, D., and Lee, H. W., “Optimization Framework for Space-Based Multi-Sensor Systems in Cislunar Space Domain Awareness,” *AAS/AIAA Astrodynamics Specialist Conference*, 2023, pp. 1–20.

[23] Lee, H. W., Shimizu, S., Yoshikawa, S., and Ho, K., “Satellite constellation pattern optimization for complex regional coverage,” *Journal of Spacecraft and Rockets*, Vol. 57, No. 6, 2020, pp. 1309–1327. <https://doi.org/10.2514/1.A34657>.

[24] Cooper, L., “Location-Allocation Problems,” *Operations Research*, Vol. 11, No. 3, 1963.

[25] Wesolowsky, G. O., “Dynamic Facility Location,” *Management Science*, Vol. 19, No. 11, 1973, pp. 1241–1548. <https://doi.org/10.1287/mnsc.19.11.1241>.

[26] Hakimi, S. L., “Optimum Distribution of Switching Centers in a Communication Network and Some Related Graph Theoretic Problems,” *Operations Research*, Vol. 13, No. 3, 1965, pp. 462–475.

[27] Cornuejols, G., Fisher, M. L., and Nemhauser, G. L., “Approximate Algorithms Linked references are available on JSTOR for this article : XeptaDcetlna] Wap,” *Management Science*, Vol. 23, No. 8, 1977.

[28] Rosenwein, M. B., *Discrete location theory*, edited by P. B. Mirchandani and R. L. Francis, John Wiley & Sons, New York, 1990, 555 pp, Vol. 24, 1994.

[29] "Simchi-Levi, D., Chen, X., and Bramel, J., *The Logic of Logistics*, Springer, New York, 2014.

[30] Wolf, G. W., "Facility location: concepts, models, algorithms and case studies. Series: Contributions to Management Science," *International Journal of Geographical Information Science*, Vol. 25, No. 2, 2011, pp. 331–333. <https://doi.org/10.1080/13658816.2010.528422>, URL <https://doi.org/10.1080/13658816.2010.528422>.

[31] Ahmadi-Javid, A., Seyed, P., and Syam, S. S., "A survey of healthcare facility location," *Computers and Operations Research*, Vol. 79, 2017, pp. 223–263. <https://doi.org/10.1016/j.cor.2016.05.018>, URL <http://dx.doi.org/10.1016/j.cor.2016.05.018>.

[32] Shimane, Y., Gollins, N., and Ho, K., "Orbital Facility Location Problem for Satellite Constellation Servicing Depots," *Journal of Spacecraft and Rockets*, Vol. 61, No. 3, 2024, pp. 808–825. <https://doi.org/10.2514/1.A35691>.

[33] Shimane, Y., Tomita, K., and Ho, K., "Strategic Regions for Monitoring Incoming Low-Energy Transfers to Low-Lunar Orbit," *Advanced Maui Optical and Space Surveillance Technologies (AMOS) Conference*, 2023.

[34] Shimane, Y., Shirane, A., and Ho, K., "Lunar Communication Relay Architecture Design via Multiperiod Facility Location Problem," *74th International Astronautical Congress*, 2023.

[35] Wesolowsky, G. O., and Truscott, W. G., "Multiperiod Location-Allocation Problem With Relocation of Facilities." *Management Science*, Vol. 22, No. 1, 1975, pp. 57–65. <https://doi.org/10.1287/mnsc.22.1.57>.

[36] Laporte, G., Nickel, S., and da Gama, F. S., *Location Science*, Springer International Publishing, 2015. <https://doi.org/10.1007/978-3-319-13111-5>, URL <http://dx.doi.org/10.1007/978-3-319-13111-5>.

[37] Nickel, S., and Saldanha-da Gama, F., *Multi-Period Facility Location*, Springer International Publishing, Cham, 2019, pp. 303–326. https://doi.org/10.1007/978-3-030-32177-2_11, URL https://doi.org/10.1007/978-3-030-32177-2_11.

[38] Hax, A., and Candea, D., *Production and Inventory Management*, Prentice-Hall, 1984. URL <https://books.google.com/books?id=Wq9vQgAACAAJ>.

[39] Tomita, K., Shimane, Y., and Ho, K., "Multi-Spacecraft Predictive Sensor Tasking for Cislunar Space Situational Awareness," *Advanced Maui Optical and Space Surveillance Technologies (AMOS) Conference*, 2023. URL <http://arxiv.org/abs/2310.04894>.

[40] Koon, W. S., Lo, M. W., Marsden, J. E., and Ross, S. D., "Low energy transfer to the Moon," *Celestial Mechanics and Dynamical Astronomy*, Vol. 81, No. 1-2, 2001, pp. 63–73. <https://doi.org/10.1023/A:1013359120468>.

[41] Belbruno, E., "Analytic estimation of weak stability boundaries and low energy transfers," *Celestial Mechanics, Dedicated to Donald Saari for his 60th Birthday*, Vol. 292, 2002, p. 17.

[42] Parker, J. S., and Anderson, R. L., *Low-Energy Lunar Trajectory Design*, Wiley, Hoboken, New Jersey, 2014.

[43] Gurobi Optimization, LLC, “Gurobi Optimizer Reference Manual,” , 2022. URL <https://www.gurobi.com>.

[44] Cplex, I. I., “V12. 1: User’s Manual for CPLEX,” *International Business Machines Corporation*, Vol. 46, No. 53, 2009, p. 157.